

Yoav Shechtman, Yonina C. Eldar, Oren Cohen, Henry N. Chapman,  
Jianwei Miao, and Mordechai Segev

# Phase Retrieval with Application to Optical Imaging

[A contemporary overview]

**T**he problem of phase retrieval, i.e., the recovery of a function given the magnitude of its Fourier transform, arises in various fields of science and engineering, including electron microscopy, crystallography, astronomy, and optical imaging. Exploring phase retrieval in optical settings, specifically when the light originates from a laser, is natural since optical detection devices [e.g., charge-coupled device (CCD) cameras, photosensitive films, and the human eye] cannot measure the phase of a light wave. This is because, generally, optical measurement devices that rely on converting photons to electrons (current) do not allow for direct recording of the phase: the electromagnetic field oscillates at rates of  $\sim 10^{15}$  Hz, which no electronic measurement device can follow. Indeed, optical measurement/detection systems measure the photon flux, which is proportional to the magnitude squared of the field, not the phase. Consequently, measuring the phase of optical waves (electromagnetic fields oscillating at  $10^{15}$  Hz and higher) involves additional complexity, typically by requiring interference with another known field, in the process of holography.

Interestingly, electromagnetic fields do have some other features that make them amenable for algorithmic phase retrieval: their far field corresponds to the Fourier transform of their near field. More specifically, given a mask that superimposes an image on a quasi-monochromatic coherent field at some plane in space, the electromagnetic field distribution at a large enough distance from that plane is given

---

Digital Object Identifier 10.1109/MSP.2014.2352673  
Date of publication: 6 April 2015

by the Fourier transform of the image multiplied by a known quadratic phase factor. Thus, measuring the far field, magnitude, and phase would facilitate recovery of the optical image (the wave field). However, as noted before, the optical phase cannot be directly measured by an electronic detector. Here algorithmic phase retrieval comes into play, offering a means for recovering the phase given the measurement of the magnitude of the optical far field and some prior knowledge.

This review article provides a contemporary overview of phase retrieval in optical imaging, linking the relevant optical physics to the signal processing methods and algorithms. Our goal is to describe the current state of the art in this area, identify challenges, and suggest future directions and areas where signal processing methods can have a large impact on optical imaging and on the world of imaging at large with applications in a variety of fields ranging from biology and chemistry to physics and engineering.

## HISTORICAL BACKGROUND

Algorithmic phase retrieval offers an alternative means for recovering the phase of optical images without requiring sophisticated measuring setups as in holography. These approaches typically rely on some advanced information to facilitate recovery. In 1952, Sayre envisioned, in the context of crystallography, that the phase information of a scattered wave may be recovered if the intensity pattern at and between the Bragg peaks of the diffracted wave is finely measured [1]. In crystallography, the material structure under study is usually periodic (a crystal); hence, the far-field information contains strong peaks reflecting the Fourier transform of the usually periodic information. Measuring the fine features in the Fourier transform enabled the recovery of the phase in some simple cases. In 1978, 26 years later, Fienup developed algorithms for retrieving phases of two-dimensional (2-D) images from their Fourier modulus and constraints such as nonnegativity and a known support of the image [2] (see Figure 1).

In the early 1980s, the idea of phase retrieval created a flurry of follow-up work, partly because those times signified great hope

for realizing an optical computer, of which phase retrieval was supposed to be a key ingredient. However, in the late 1980s and early 1990s, with the understanding that an optical computer is unrealistic, the interest in algorithmic phase retrieval diminished. Toward the end of the millennium, optical phase retrieval started to come back into contemporary optics research with the interest arising from a completely different direction: the community of researchers experimenting with X-ray imaging, where new X-ray sources (undulators and synchrotrons) were developed. The widespread interest in this field was mainly generated by the first experimental recording and reconstruction of a continuous diffraction pattern (Fourier magnitude squared) of a noncrystalline (non-periodic) test object by Miao et al. in 1999 [3].

The reasons for the revival of optical phase retrieval in 1999 were actually quite subtle. One goal of optical imaging systems is to increase resolution, i.e., to image smaller and smaller features. However, as proved by Abbe's work in 1873, the highest attainable resolution in diffraction imaging (the so-called diffraction limit) is comparable to the wavelength of the light. For visible light, this diffraction limit corresponds to fractions of microns. Consequently, features on the molecular scale cannot be viewed with visible light in a microscope. One could argue then, why not simply use electromagnetic waves of a much shorter wavelength, say, in the hard X-ray regime, where the wavelength is comparable to atomic resolution? The reason is that lens-like devices and other optical components in this spectral region suffer from very large aberrations and are very difficult to make because refractive indices of materials in this wavelength regime are close to one. On the other hand, algorithmic phase retrieval is of course not limited by the quality of lenses; however, it requires very low noise detectors.

An additional problem is that as resolution is improved (i.e., as voxel elements in the recovered image are smaller in size), the number of photons per unit area must obviously increase to provide a reasonable signal-to-noise ratio (SNR). This means that the required exposure time to obtain a given signal level must increase as  $(1/d)^4$ , with  $d$  being the resolution length, assumed

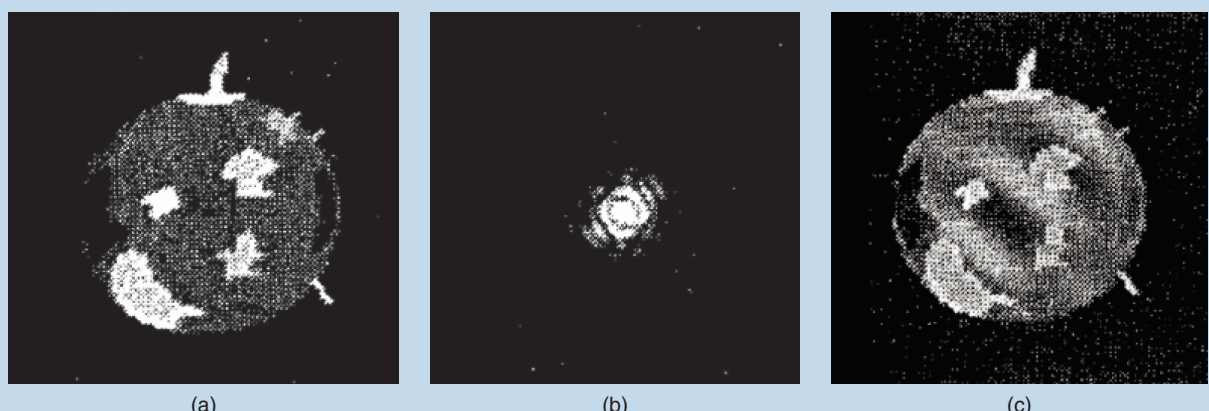


**[FIG1]** A numerical 2-D phase-retrieval example adapted from Fienup's 1978 paper [2]: (a) test object, (b) Fourier magnitude, and (c) reconstruction results [using hybrid input-output (HIO)—see Figure 3(b) for details]. (Images used with permission from [2].)

to be larger than atomic scales [4]. This, in turn, creates another problem: X-ray photons are highly energetic. The atomic cross section for photoabsorption is usually much higher than for elastic scattering, meaning that for every photon that contributes to the diffraction pattern (the measured Fourier magnitude), a considerable greater number of photons are absorbed by the sample. This energy dissipates in the sample first by photoionization and the breakage of chemical bonds, followed by a cascade of collisional ionization by free electrons and, at longer timescales, a destruction of the sample due to radiolysis, heating, or even ablation of the sample. Such radiation damage hinders the ability to recover the structure of molecules: the measured far-field intensity (Fourier magnitude) would reflect the structural damages, rather than providing information about the true molecular structure.

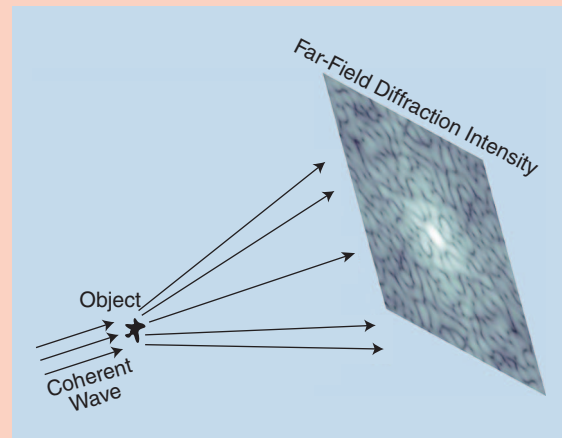
A solution to this problem was suggested by Solem and Chapline in the 1980s. They proposed to record images with pulses that are shorter than the timescale for the X-ray damage to occur. They predicted that picosecond pulses would be required to image at nanometer-length scales [5]. Toward the late 1980s, with the growing promise in constructing X-ray lasers that generate ultra-short pulses on the femtosecond scale, it was suggested that such pulses could even outrun damage processes at atomic length scales [6]. However, forming a direct image in this way would still require high-quality optical components (lenses and mirrors) in the X-ray regime, which do not currently exist. This is because creating lenses for the hard X-ray wavelength regime requires fabrication at picometer resolution, much smaller even than the Bohr radius of atoms. Likewise, while mirrors for X-rays do exist, their best resolution is on the scale of many nanometers, much larger than the features one would want to resolve in the imaging of molecules, for example.

The difficulties outlined earlier in direct X-ray imaging leave no choice but to use alternative methods to recover the structure of nanometric samples. Here is where phase retrieval can make its highest impact. Placing an area detector far enough from the sample to record the far-field diffraction intensity (which is approximately proportional to the squared magnitude of the Fourier transform of the image if the coherence length of the X-ray wave is larger than the sample size [7], [145]), together with appropriate constraints on the support of the sample, enable the recovery of the image at nanometric resolution. Indeed, the phase information has been shown numerically and experimentally to be retrieved in this fashion in various examples [2], [8]–[12].

The combination of X-ray diffraction, oversampling, and phase retrieval has launched the currently very active field called *coherent diffractive imaging* (CDI) [3]. In CDI, an object is illuminated with a coherent wave and the far-field diffraction intensity pattern (corresponding to the Fourier magnitude of the object) is measured. The problem then is to recover the object from the measured far-field intensity (see “Coherent Diffractive Imaging” and Figure S1). Since its first experimental demonstration, CDI has been applied to image a wide range of samples using synchrotron radiation [13]–[15], X-ray free-electron lasers (XFELs) [16], [17], high harmonic generation [18]–[20], soft X-ray laser [21], optical laser [22], and electrons [23], [24]. Recent reviews on the development and implementation

## COHERENT DIFFRACTIVE IMAGING

In the basic CDI setup (forward scattering), an object is illuminated by a quasi-monochromatic coherent wave and the diffracted intensity is measured (Figure S1). When the object is small and the intensity is measured far away, the measured intensity is proportional to the magnitude of the Fourier transform of the wave at the object plane with appropriate spatial scaling.



**[FIGS1]** A forward-scattering CDI setup: a coherent wave diffracts from an object (the sought information) and produces a far-field intensity pattern corresponding to the magnitude of the Fourier transform of the object.

In optics terms, when the Fresnel number is small ( $N_F = (a^2/\lambda d) \ll 1$ , where  $a$  is a radius confining the object in the object plane,  $d$  is the distance between the object and the measured intensity plane, and  $\lambda$  is the wavelength of the light), the relationship between the measured intensity  $I_{\text{out}}$  and the wave at the object plane  $E_{\text{in}}$  is given by [37]

$$I_{\text{out}}(x, y) \propto \left| \hat{E}_{\text{in}}\left(\frac{x}{\lambda d}, \frac{y}{\lambda d}\right) \right|^2$$

with  $\hat{E}_{\text{in}} = \mathcal{F}\{E_{\text{in}}\}$  and  $\mathcal{F}$  denoting the Fourier transform. Once the far-field intensity is measured, the goal is to recover  $E_{\text{in}}$  (which is equivalent to recovering the object) from  $I_{\text{out}}$ . This requires solving the phase-retrieval problem, which is attempted using an algorithm such as the ones described in this article.

of phase-retrieval algorithms for the specific application of CDI were written by Marchesini [9], Thibault and Elser [25], and Nugent [26]. Presently, one of the most challenging problems in CDI is three-dimensional (3-D) structural determination of large protein molecules [6]. There has been ongoing progress toward this goal over the past decade; see, e.g., [16], [17], [27], and [28].

Another research field where phase retrieval plays an important role is astronomy, where the objects are usually distant stars, which are optically incoherent sources. In such cases of incoherent waves, the phase is stochastic; hence, the optical signal is the

intensity of the light (amplitude of the complex field squared). This has important implications on algorithmic phase retrieval in terms of the assumptions that can be made on the signal (e.g., nonnegativity). One application of phase retrieval in astronomical measurements is for adaptive optics-based aberration correction, caused either by atmospheric turbulence or by imperfections in the optical imaging system [29]–[31]. Phase retrieval is also used in speckle interferometry [32], [33], a method to obtain information and later images [34], [35] beyond the diffraction limit of the (telescopic or alike) imaging system. As phase retrieval plays a major role in astronomy, there exist several detailed reviews from this perspective [31], [33], [36].

From a theoretical and algorithmic point of view, phase retrieval is a difficult problem, in many cases lacking a unique solution. Furthermore, even with the existence of a unique solution, there is not necessarily a guarantee that it can be found algorithmically. Nevertheless, as reasoned earlier, phase-retrieval algorithms and applications have benefited from a surge of research in recent years, in large part due to various new imaging techniques in optics. This trend has begun impacting the signal processing community as well—the past few years have witnessed growing interest within this community in developing new approaches to phase retrieval by using the tools of modern optimization theory [38], [39]. More recent work has begun exploring connections between phase retrieval and structure-based information processing [40]–[45]. For example, it has been shown that, by exploiting the sparsity of many optical images, one can develop powerful phase-retrieval methods that allow for increased resolution considerably beyond Abbe's diffraction limit, resolving features smaller than one-fifth of the wavelength [45]. The relationship between the fields of sparsity and optical imaging has led to an important generalization of the basic principles of sparsity-based reconstruction to nonlinear measurement systems [41], [44], [46]–[53]. Here too, optics played an important role in signal processing: since the phase-retrieval problem is inherently nonlinear (i.e., the signal is related to the measurements nonlinearly), employing sparsity-based concepts in phase retrieval required modifications to the linear sparsity-based algorithms known from the field of compressed sensing [54]. We believe that this field will grow steadily in the next few years, with rapid development of coherent X-ray sources worldwide [55], [56] and more researchers contributing to the theory, algorithms, and practice of nonlinear sparse recovery.

## MATHEMATICAL FORMULATION

### PROBLEM FORMULATION

Consider the discretized one-dimensional (1-D) real-space distribution function of an object:  $\mathbf{x} \in \mathbb{C}^N$  (extension of the formulation to higher dimensions is straightforward). In CDI, for

## THE RELATIONSHIP BETWEEN THE FIELDS OF SPARSITY AND OPTICAL IMAGING HAS LED TO AN IMPORTANT GENERALIZATION OF THE BASIC PRINCIPLES OF SPARSITY-BASED RECONSTRUCTION TO NONLINEAR MEASUREMENT SYSTEMS.

example, this corresponds to the transmittance function of the object. The fact that  $\mathbf{x}$  is generally complex corresponds physically to the fact that the electromagnetic field emanating from different points on the object has not only magnitude but also phase (as is always the case, for example, when 3-D objects are illuminated and light is reflected from points at different planes). The 1-D discrete Fourier transform (DFT) of  $\mathbf{x}$  is given by

$$X[k] = \sum_{n=0}^{N-1} x[n] e^{-j2\pi \frac{kn}{N}}, \quad k = 0, 1, \dots, N-1. \quad (1)$$

The term *oversampled DFT* used in this article will refer to an  $M$ -point DFT of  $\mathbf{x} \in \mathbb{C}^N$  with  $M > N$

$$X[k] = \sum_{n=0}^{N-1} x[n] e^{-j2\pi \frac{kn}{M}}, \quad k = 0, 1, \dots, M-1. \quad (2)$$

The recovery of  $\mathbf{x}$  from measurement of  $\mathbf{X}$  can be achieved by simply applying the inverse-DFT operator. Writing  $X[k] = |X[k]| \cdot e^{j\phi[k]}$ , the Fourier phase-retrieval problem is to recover  $\mathbf{x}$  when only the magnitude of  $\mathbf{X}$  is measured, i.e., to recover  $x[n]$  given  $|X[k]|$ . Since the DFT operator is bijective, this is equivalent to recovering the phase of  $X[k]$ , i.e.,  $\phi[k]$ —hence the term *phase retrieval*. Denote by  $\hat{\mathbf{x}}$  the vector  $\mathbf{x}$  after padding with  $N-1$  zeros. The autocorrelation sequence of  $\hat{\mathbf{x}}$  is then defined as

$$g[m] = \sum_{i=\max(1, m+1)}^N \hat{x}_i \overline{\hat{x}_{i-m}}, \quad m = -(N-1), \dots, N-1. \quad (3)$$

It is well known that the DFT of  $g[m]$ , denoted by  $G[k]$ , satisfies  $G[k] = |X[k]|^2$ . Thus, the problem of recovering a signal from its Fourier magnitude is equivalent to recovering a signal from its autocorrelation sequence.

Continuous phase retrieval can be defined similarly to its discrete counterpart as the recovery of a 1-D signal  $f(x)$  from its continuous Fourier magnitude

$$|F(\nu)| = \left| \int_{\mathbb{R}} f(x) \exp(-j2\pi\nu x) dx \right|.$$

Many objects of interest, such as electromagnetic fields, are usually described by continuous functions. However, since the data acquisition is digitized (by CCD cameras and alike), and the processing is done digitally, we mostly treat the discrete case here.

The Fourier phase-retrieval problem is as a special case of the more general phase-retrieval problem, where we are given measurements

$$y_k = |\langle \mathbf{a}_k, \mathbf{x} \rangle|^2, \quad k = 1, \dots, M, \quad (4)$$

with  $\mathbf{a}_k$  denoting the measurement vectors. In discrete 1-D Fourier phase retrieval, the measurement vectors correspond to  $\mathbf{a}_k[n] = e^{-j2\pi(kn)/M}$ . For mathematical analysis, it is often easier to

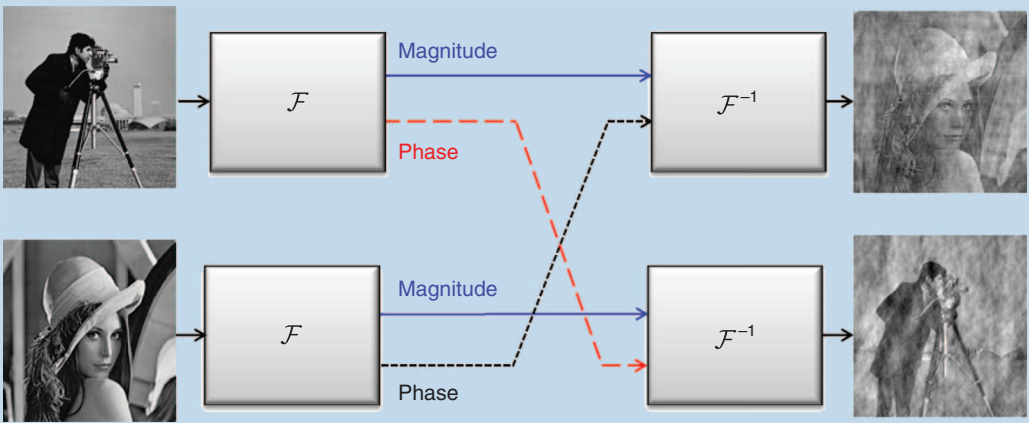


**[FIG2]** The importance of Fourier phase. Two images, a cameraman and Lenna, are Fourier transformed. After swapping their phases, they are inverse Fourier transformed. The result clearly demonstrates the importance of phase information for image recovery.

treat the case where the measurements are random (i.e.,  $a_k$  are random vectors), as this allows uniqueness guarantees that are otherwise hard to obtain [38], [50], [57]–[59]. Nevertheless, more structured measurements have also been investigated [60].

Before proceeding to the mathematical methodology, it is important to highlight the significance of knowing the Fourier phase. In fact, it is well known that knowledge of the Fourier phase is crucial in recovering an object from its Fourier transform [61]. Many times the Fourier phase contains more information than the Fourier magnitude, as can be seen in the synthetic example shown in Figure 2. The figure shows the result of the following numerical experiment: two images (that of a cameraman and a woman named Lenna) are Fourier transformed. The phases of their transforms are swapped and, subsequently, they are inverse Fourier transformed. It is evident, for this quite arbitrary example, that the Fourier phase contains a significant amount of information about the images. In crystallography, this phenomenon is the source of genuine concern of phase bias of molecular models (such as those used in molecular replacement) in refined structures.

In the remainder of this section, we discuss uniqueness of the phase-retrieval problem, i.e., under what conditions the solution to the phase problem is unique. It is worth noting that, while the discussion of theoretical uniqueness guarantees is important and interesting, the lack of such guarantees does not prevent practical applications from producing excellent reconstruction results in many settings.

## UNIQUENESS

### FOURIER MEASUREMENTS

The recovery of a signal from its Fourier magnitude alone, in general, does not yield a unique solution. This section will review the main existing theoretical results regarding phase-retrieval uniqueness.

First, there are so-called trivial ambiguities that are always present. The following three transformations (or any combination of them) conserve Fourier magnitude:

- 1) global phase shift:  $x[n] \Rightarrow x[n] \cdot e^{j\phi_0}$
- 2) conjugate inversion:  $x[n] \Rightarrow \overline{x[-n]}$
- 3) spatial shift:  $x[n] \Rightarrow x[n + n_0]$ .

Second, there are nontrivial ambiguities, the situation of which varies for different problem-dimensions. In the 1-D setting, there is no uniqueness—i.e., there are multiple 1-D signals with the same Fourier magnitude. Even if the support of the signal is bounded within a known range, uniqueness does not exist [62]. Any pair of 1-D signals having the same autocorrelation function yields the same Fourier magnitude, as the two are connected by a Fourier transform. Consider, for example, the two vectors  $u = [1 \ 0 \ -2 \ 0 \ -2]^T$  and  $v = [(1 - \sqrt{3}) \ 0 \ 1 \ 0 \ (1 + \sqrt{3})]^T$ . Both of these vectors have the same support and yield the same autocorrelation function  $g[m] = [-2, 0, 2, 0, 9, 0, 2, 0, -2]$ . Therefore, they are indistinguishable by their Fourier magnitude, even though they are not trivially equivalent.

For higher dimensions (2-D and above), Bruck and Sodin [63], Hayes [64], and Bates [65] have shown that, with the exception of a set of signals of measure zero, a real  $d \geq 2$  dimensional signal with support  $N = [N_1 \dots N_d]$ , i.e.,  $x[n_1, \dots, n_d] = 0$  whenever  $n_k < 0$  or  $n_k \geq N_k$  for  $k = 1, \dots, d$  is uniquely specified by the magnitude of its continuous Fourier transform, up to the trivial ambiguities mentioned earlier. Furthermore, the magnitude of the oversampled  $M$  point DFT sequence of the signal, with  $M \geq 2N - 1$  (where the inequality holds in every dimension), is sufficient to guarantee uniqueness. The problematic set of signals that are not uniquely defined by their Fourier magnitudes are those having a reducible Z transform: denoting the  $d$ -dimensional Z transform of  $x$  by  $X(z_1, \dots, z_d) = \sum_{n_1} \dots \sum_{n_d} x[n_1, \dots, n_d] z_1^{-n_1} \dots z_d^{-n_d}$ ,  $X(z)$  is said to be reducible if it can be written as  $X(z) = X_1(z) X_2(z)$ , where  $X_1(z)$  and  $X_2(z)$  are both polynomials in  $z$  with degree  $p > 0$ . It is important to note that, in practice, for typical images, a number of samples smaller than  $2N - 1$  is many times sufficient (even  $M \geq 2^{1/D} N$  can work, where  $D$  is the dimension [66]); however, the exact guarantees relating the number of samples to the type of images remains an open question.

[TABLE 1] PHASE RETRIEVAL—UNIQUENESS.

FOURIER MEASUREMENT	1-D	NO UNIQUENESS [62]
	$\geq 2D$	UNIQUENESS FOR REAL NONREDUCIBLE SIGNALS. REQUIRES OVERSAMPLING BY $\approx 2$ [64]
	$k$ -SPARSE 1-D	UNIQUENESS FOR SIGNAL WITH COLLISION-FREE AUTOCORRELATION, (AND $K \neq 6$ ) [69] $M$ FOURIER MAGNITUDE MEASUREMENTS ARE SUFFICIENT, FOR A PRIME $M \geq k^2 - k + 1$ [70]
GENERAL MEASUREMENTS	REAL SIGNAL $R^N$	SATISFYING THE COMPLEMENT PROPERTY IS NECESSARY AND SUFFICIENT. $2N-1$ FULL-SPARK RANDOM MEASUREMENTS GUARANTEE UNIQUENESS WITH HIGH PROBABILITY [40]
	REAL SIGNAL $R^N$ (NOISY)	$N \log(N)$ MEASUREMENTS (OR $k \log(N)$ MEASUREMENTS IN THE $k$ -SPARSE CASE) ARE SUFFICIENT FOR STABLE UNIQUENESS [50]
	COMPLEX SIGNAL $C^N$	CONJECTURE: $4N-4$ GENERIC MEASUREMENTS ARE SUFFICIENT [43]

Additional prior information about the signal, other than its support, can be incorporated and will naturally improve the conditioning of the problem. For example, knowledge of the Fourier phase sign (i.e., a single bit of phase information) has been shown [67] to yield uniqueness with some restrictions on the signal (specifically that the signal is real and its Z transform has no zeros on the unit circle). A different, popular, type of prior knowledge that has been used recently in various applications [54], [68] is that the signal  $x \in \mathbb{C}^N$  is sparse—i.e., contains only a small number  $k$  of nonzero elements, with  $k \ll N$ . The exact locations and values of the nonzero elements are not known a priori. In this case, it has been shown [69] that knowledge of the full autocorrelation sequence of a 1-D  $k$ -sparse real signal  $x$  is sufficient to uniquely define  $x$  as long as  $k \neq 6$  and the autocorrelation sequence is collision free. A vector  $x$  is said to have a collision-free autocorrelation sequence if  $x[i] - x[j] \neq x[k] - x[l]$ , for all distinct  $i, j, k, l \in \{1, \dots, N\}$  that are the locations of distinct nonzero values in  $x$ . In addition, under these conditions, only  $M$  Fourier magnitude measurements are sufficient to uniquely define the autocorrelation sequence and, therefore, the signal  $x$ , as long as  $M$  is prime and  $M \geq k^2 - k + 1$  [70]. An interesting perspective relating phase retrieval to the Turnpike problem, for example, reconstructing a set of integers from their pairwise distances, is presented in [71]. Using this approach, the authors prove uniqueness with high probability for random signals having a nonperiodic support.

## GENERAL MEASUREMENTS

Considering inner products with general non-Fourier (typically random) measurement vectors allows simpler derivation of theoretical guarantees. There have been several theoretical results relating the number and the nature of the measurements that are required for uniqueness, mostly dealing with random measurement vectors. The work of Balan [40] implies that, for real signals in  $\mathbb{R}^N$ ,  $2N-1$  random measurements are needed, provided that they are full spark, i.e., that every subset of  $N$  measurement vectors spans  $\mathbb{R}^N$  [43]. This result was later extended to the complex case [43], where it is conjectured that  $4N-4$  generic measurements, as defined in [43], are sufficient for bijectivity. In terms of stability, i.e., when the measurements are noisy, it is shown in [50] that on the order of  $N \log(N)$  measurements [or  $k \log(N)$ ] measurements in the

$k$ -sparse case] are sufficient for stable uniqueness. Furthermore, minimizing the (nonconvex) least-squares objective:  $\sum |y_i^2 - |\langle a_i, x \rangle|^2|^p$ , with  $1 < p \leq 2$ , yields the correct solution under these conditions [50]. For the noiseless case, any  $k$ -sparse vector in  $\mathbb{R}^N$  has been shown to be uniquely determined by  $4k-1$  random Gaussian intensity measurements with high probability [70].

To study the injectivity of general (i.e., not necessarily random) measurements, the complement property was introduced in [40] for the real case. An extension was presented in [43] for the complex setting. A set of measurement vectors  $\{a_i\}_{i=1}^M$  with  $a_i \in \mathbb{R}^N$  satisfies the complement property if for every  $S \subseteq \{1, \dots, M\}$ , either  $\{a_i\}_{i \in S}$  or  $\{a_i\}_{i \in S^c}$  span  $\mathbb{R}^N$ . It has been shown in [40] that the mapping constructed by  $y_i = |\langle a_i, x \rangle|$ ,  $i = 1, \dots, N$  is injective if and only if the measurement set satisfies the complement property. This poses a lower limit on the number of necessary measurements  $M > 2N-1$ .

The results reviewed in this section are summarized in Table 1. In addition, there is a large amount of work on phase-retrieval uniqueness under different conditions, e.g., when the phase is known only approximately [72] or from redundant masked Fourier measurements [42], [73].

## ALGORITHMS

Despite the uniqueness guarantees, no known general solution method exists to actually find the unknown signal from its Fourier magnitude given the other constraints. Over the years, several approaches have been suggested for solving the phase-retrieval problem, with the popular ones being alternating projection algorithms [2], [74], [75]. In addition, to help regularize the phase-retrieval problem, different imaging techniques were suggested that yield better behaved imaging models. For example, using exposures with different masks (e.g., the phase diversity method for aberration correction by adaptive optics [29], and also more recently [73]), or obtaining images at different propagation planes [31], [76], [77]. Another method to obtain additional information is scanning CDI (also termed *ptychography*) [78]–[80], which uses several different illumination patterns to obtain coherent diffraction images. Using such a modified imaging setup is then followed by applying an appropriate algorithm, performing the phase retrieval.

There are many existing approaches for phase retrieval. In this section, we focus on common general algorithms (see the

“General Algorithms” section) and sparsity-based methods, i.e., techniques exploiting prior knowledge in the form of signal sparsity (see the “Sparsity-Based Algorithms” section). We also discuss the transport-of-intensity equation (TIE) [81]–[83], which considers the recovery of an object’s phase from several defocused intensity images.

## GENERAL ALGORITHMS

The general phase-retrieval problem we wish to solve can be formulated as the following least squares problem or empirical risk minimization:

$$\min_x \sum_{k=1}^M (y_k - |\langle a_k, x \rangle|^2)^2, \quad (5)$$

with  $y$  being the measurements and  $a_k$  being the measurement vectors defined in (4). In general, we can replace the square in the objective by any power  $p$ . Unfortunately, this is a nonconvex problem, and it is not clear how to find a global minimum even if one exists. In this section, we describe several approaches that have been suggested to deal with this problem and types of prior information that can be incorporated into these methods to increase the probability of convergence to the true solution.

## ALTERNATING PROJECTIONS

The most popular class of phase-retrieval methods is based on alternate projections. These methods were pioneered by the work of Gerchberg and Saxton (GS) [74], dealing with the closely related problem of recovering a complex image from magnitude measurements at two different planes—the real (imaging) plane and Fourier (diffraction) plane. The original GS algorithm consists of iteratively imposing the real- and Fourier-plane constraints, such as the measured real-space magnitude  $|x[n]|$ , and Fourier magnitude  $|X[k]|$ , as illustrated in Figure 3(a). The GS iterations are described in Algorithm 1. The recovery error, defined as  $E_i = \sum_k |Z_i[k] - X[k]|^2$ , is easily

shown to be monotonically nonincreasing with  $i$  [75]. Despite this fact, recovery to the true solution is not guaranteed, as the algorithm can converge to a local minimum.

---

### Algorithm 1: The GS algorithm.

---

**Input:**  $|x[n]|, |X[k]|, \epsilon$

$|x[n]|$ -Real-space magnitude

$|X[k]|$ -Fourier magnitude

$\epsilon$ -Error threshold

**Output:**  $z[n]$ - a vector that conforms with both magnitude constraints, i.e.,  $|z[n]| = |x[n]|$ , and  $|Z[k]| = |X[k]|$ , where  $Z[k]$  is the DFT of  $z[n]$

**Initialization:** Choose initial  $z_0[n] = |x[n]| \exp(\phi[n])$  (e.g., with a random  $\phi[n]$ )

**General Step:** ( $i = 1, 2, \dots$ ):

- 1) Fourier transform  $z_i[n]$  to obtain  $Z_i[k]$
- 2) Keep current Fourier phase, but impose Fourier magnitude constraint:  $Z_i[k] = |X[k]| \cdot Z_i[k] / |Z_i[k]|$ .
- 3) Inverse Fourier transform  $Z_i[k]$  to obtain  $z'_i[n]$
- 4) Keep current real-space phase, but impose real-space magnitude constraint:  $z_{i+1}[n] = |x[n]| \cdot z'_i[n] / |z'_i[n]|$
- 5) Go to 1

Until  $E_i = \sum_k |Z_i[k] - X[k]|^2 \leq \epsilon$

---

Extending the GS projection ideas further, in 1978 Fienup [2] suggested a modified version, in which the real-space magnitude constraints are replaced by other types of constraints, in addition to consistency with the measured Fourier magnitude. The real-space constraints may be, e.g., nonnegativity, a known signal support, i.e.,  $x[i] = 0$  for all  $i > N_0$ , where  $N_0$  is known (or approximately known), or both. The basic framework of the Fienup methods is similar to GS—in fact, the first three steps are identical. Step 4, however, replaces imposing the real-space magnitude constraint by applying a correction to the real-space

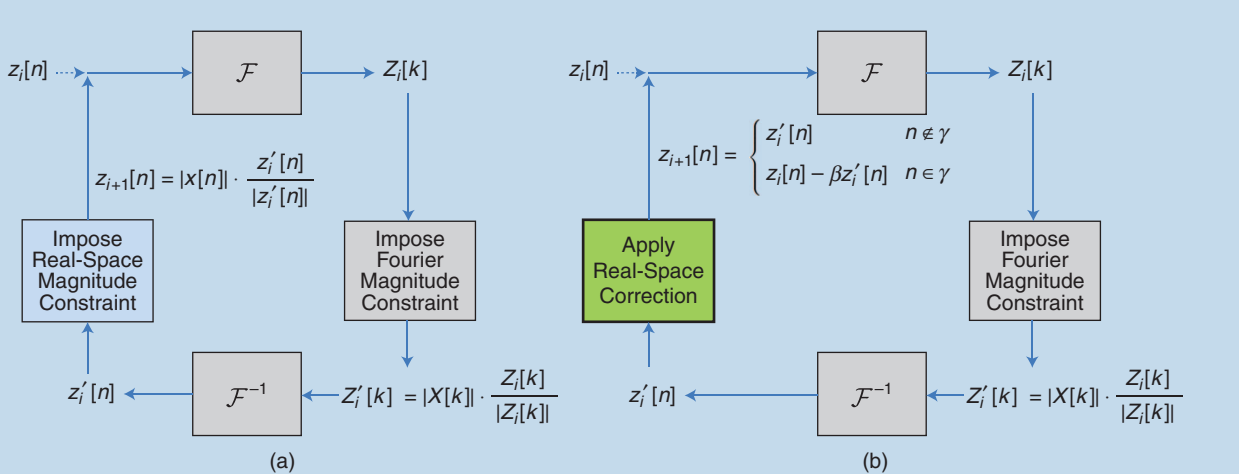


[FIG3] The block diagrams of (a) the GS algorithm and (b) the Fienup HIO algorithm. The algorithms differ in their fourth (colored) step.

estimate. Some possible variants to this step were also suggested [75]. Here, we describe the one most commonly used, referred to as the *hybrid input-output (HIO) method*, which consists of the following correction step:

4) Obtain  $z_{i+1}[n]$  by applying a correction to the real-space image estimate:

$$z_{i+1}[n] = \begin{cases} z'_i[n], & n \notin \gamma \\ z_i[n] - \beta z'_i[n], & n \in \gamma, \end{cases} \quad (6)$$

with  $\beta$  being a small parameter and  $\gamma$  being the set of indices for which  $z'_i[n]$  violates the real-space constraints.

The real-space constraint violation may be a support violation (e.g., a signal is nonzero where it should be zero) or a nonnegativity violation.

The Fienup algorithm is represented schematically in Figure 3(b). There is no proof that the HIO algorithm converges. It is also known to be sensitive to the accuracy of the prior information (e.g., the real-space support needs to be tightly known, especially in the complex signal case [84]). Nonetheless, in practice, the simple HIO-based techniques are commonly used in optical phase-retrieval applications such as CDI [85], [86]. Other variants of the correction step include the input–output method, and the output–output method [75], corresponding respectively to

$$\begin{aligned} z_{i+1}[n] &= \begin{cases} z_i[n], & n \notin \gamma \\ z_i[n] - \beta z'_i[n], & n \in \gamma, \end{cases} \\ z_{i+1}[n] &= \begin{cases} z'_i[n], & n \notin \gamma \\ z'_i[n] - \beta z_i[n], & n \in \gamma. \end{cases} \end{aligned} \quad (7)$$

An important feature of the HIO algorithm is its empirical ability to avoid local minima and converge to a global minimum for noise-free oversampled diffraction patterns. However, when there is high noise present in the diffraction intensity, HIO suffers from several limitations. First, the algorithm sometimes becomes stagnant and fails to converge to a global minimum. Second, a support has to be predefined. Third, the image oscillates as a function of the iteration. Over the years, various algorithms have been developed to overcome these limitations, including the combination of HIO and the error-reduction (ER) algorithm [75], difference map [8], hybrid projection reflection [10], guided HIO (GHIO) [87], relaxed averaged alternating reflectors (RAAR) [11], noise robust (NR)-HIO [88], and oversampling smoothness (OSS) [12].

As an example, the recently proposed OSS algorithm exhibits improved performance over HIO and its variants in many settings. OSS is based on Fienup iterations with an added smoothing Gaussian filter applied to the off-support region in the real-space object in each iteration. The fourth step in HIO is replaced by

$$\begin{aligned} z''[n] &= \begin{cases} z'_i[n], & n \notin \gamma \\ z_i[n] - \beta z'_i[n], & n \in \gamma, \end{cases} \\ z_{i+1}[n] &= \begin{cases} z''[n], & n \notin \gamma \\ \mathcal{F}\{Z''_i[k]W[k]\}, & n \in \gamma, \end{cases} \end{aligned}$$

where  $W[k]$  is a Gaussian function with its variance decreasing with iterations. A quantitative comparison for a specific example between OSS and HIO can be found in the section “Quantitative Comparison of Alternating-Projection Algorithms.” For a comparison and numerical investigation of several alternate projection algorithms, see, e.g., [9] and [12].

The performance of Fienup methods is dependent on the initial points. Therefore, it is possible and recommended to try several initializations. In [58], the authors consider a clever method for initial point selection and show that for the random Gaussian measurement case, the resulting iterations yield a solution arbitrarily close to the true vector.

Analyses of iterative phase-retrieval algorithms from a convex optimization perspective can be found in [10] and [89]–[93]. In [91], the authors study the ER algorithm by viewing it as an iterated projections algorithm onto nonconvex sets. In [10] and [92], it is shown that the HIO method can be interpreted within different optimization frameworks depending on the constraints enforced. For example, given a support constraint, HIO coincides with the Douglas–Rachford algorithm for  $\beta = 1$  [94], [95]. In [10], it is shown that under the same constraint, in the more general case of  $\beta \neq 1$ , HIO can be formulated in terms of projections and reflections. This representation, however, no longer holds when nonnegativity restrictions are added.

## SEMICONVEX PROGRAMMING ALGORITHMS

An alternative recently developed to solve the phase-retrieval problem is based on semidefinite relaxation [39], [46], [57], [96]. The method relies on the observation that (4) describes a set of quadratic equations that can be rewritten as linear equations in a higher dimension. Specifically, define the  $N \times N$  matrix  $\mathbf{X} = \mathbf{x}\mathbf{x}^*$ . The measurements (4) are then linear in  $\mathbf{X}$

$$y_k = |\langle \mathbf{a}_k, \mathbf{x} \rangle|^2 = \mathbf{x}^* \mathbf{a}_k \mathbf{a}_k^* \mathbf{x} = \mathbf{x}^* \mathbf{A}_k \mathbf{x} = \text{Tr}(\mathbf{A}_k \mathbf{x}), \quad (8)$$

where  $\mathbf{A}_k = \mathbf{a}_k \mathbf{a}_k^*$ . Our problem is then to find a matrix  $\mathbf{X} = \mathbf{x}\mathbf{x}^*$  that satisfies (8). The constraint  $\mathbf{X} = \mathbf{x}\mathbf{x}^*$  is equivalent to the requirement that  $\mathbf{X}$  has rank 1, and is positive semidefinite, which we denote by  $\mathbf{X} \succeq 0$ . Therefore, finding a vector  $\mathbf{x}$  satisfying (4) can be formulated as

$$\begin{aligned} &\text{find } \mathbf{X} \\ &\text{s.t. } y_k = \text{Tr}(\mathbf{A}_k \mathbf{X}), \quad k = 1, \dots, M, \\ &\quad \mathbf{X} \succeq 0, \\ &\quad \text{rank}(\mathbf{X}) = 1. \end{aligned} \quad (9)$$

Equation (9) is equivalent to the following rank minimization problem:

$$\begin{aligned} &\min \text{rank}(\mathbf{X}) \\ &\text{s.t. } y_k = \text{Tr}(\mathbf{A}_k \mathbf{X}), \quad k = 1, \dots, M, \\ &\quad \mathbf{X} \succeq 0. \end{aligned} \quad (10)$$

Unfortunately, rank minimization is a hard combinatorial problem. However, since the constraints in (10) are convex (in fact linear), one might try to relax the minimum rank objective, for

example, by replacing it with minimization of  $\text{Tr}(\mathbf{X})$ . This approach is referred to as *PhaseLift* [39]. Alternatively, one may use the log-det reweighted rank minimization heuristic suggested in [97], which is the approach followed in [38] and [46]. In [38], it is shown that PhaseLift yields the true vector  $\mathbf{x}$  with large probability when the measurements are random Gaussian and  $M \sim O(N \log N)$ .

An interesting approach is taken in [57], where  $\mathbf{x}$  is separated into an amplitude component and a phase component, and only the phase is optimized. This approach yields several variations of existing methods, notably *PhaseCut* [57], which is a relaxation of the *MaxCut* algorithm [98] obtained by dropping the rank constraint.

The semidefinite programming (SDP) approach requires matrix lifting, i.e., replacing the sought vector with a higher-dimensional matrix, followed by solving a high-dimensional problem. It is, therefore, in principle, more computationally demanding than the alternating projection approaches, or greedy methods, which will be discussed in the section “Greedy Methods with Sparsity Prior.” In addition, in general, there is no guarantee that the rank minimization process will yield a rank-1 matrix or that the true solution will be found even if there is a unique solution.

### SPARSE LINEAR PROBLEMS

Finding sparse solutions to sets of equations is a topic that has drawn much attention in recent years [54], [68], [105], [106]. Consider the linear system

$$\mathbf{y} = \mathbf{Ax} \quad (\text{S1})$$

with  $\mathbf{y}$  being a set of  $M$  linear measurements,  $\mathbf{A}$  being an  $M \times N$  measurement matrix, and  $\mathbf{x}$  being the unknown length— $N$  vector. When the system is underdetermined (i.e.,  $M < N$ ), there are infinitely many possible solutions  $\mathbf{x}$ . A key result of the theory of sparse recovery is that adding the constraint that  $\mathbf{x}$  is sparse, i.e., contains only a few nonzero entries guarantees a unique solution to (S1), under general conditions on  $\mathbf{A}$ . One such condition is based on the coherence of  $\mathbf{A}$  [107]

$$\|\mathbf{x}\|_0 \leq \frac{1}{2} \left( 1 + \frac{1}{\mu} \right), \quad (\text{S2})$$

with  $\|\mathbf{x}\|_0$  being the number of nonzero entries in  $\mathbf{x}$ , and the coherence defined by

$$\mu = \max_{i,j} \frac{|\langle \mathbf{A}_i, \mathbf{A}_j \rangle|}{\|\mathbf{A}_i\| \cdot \|\mathbf{A}_j\|}. \quad (\text{S3})$$

Here, we denote by  $\mathbf{A}_i$  the  $i$ th column of  $\mathbf{A}$ , and by  $\|\mathbf{A}_i\|$  its Euclidean norm.

Under (S2), one can find the unique solution to (S1) by solving

$$\min_{\mathbf{x}} \|\mathbf{x}\|_0 \quad \text{s.t. } \mathbf{y} = \mathbf{Ax}. \quad (\text{S4})$$

Unfortunately, (S4) is an NP-hard combinatorial problem. However, many methods have been developed to approximately

### TRANSPORT OF INTENSITY

The TIE approach is a method that solves the known propagation equation of the electromagnetic field to recover the phase at some plane  $z_0$ , from several intensity measurements in the vicinity of that plane. Specifically, in the case of light propagation under the paraxial approximation (i.e., only small angles from the optical axis are considered, implying that the light field varies slowly on the scale of the optical wavelength), the TIE is

$$\frac{2\pi}{\lambda} \frac{\partial I}{\partial z} = -\nabla I \cdot \nabla \phi - I \Delta \phi, \quad (\text{11})$$

where  $I(x, y, z_0)$  is the intensity distribution in plane  $z_0$ ,  $\lambda$  is the wavelength of a monochromatic field,  $\nabla = (\partial_x, \partial_y)$  is the transverse gradient,  $\Delta = \nabla^2 = \partial_x^2 + \partial_y^2$  is the 2-D Laplacian, and  $\phi(x, y, z_0)$  is the phase to be recovered. Recovering  $\phi$  amounts to solving the partial differential equation (11). This can be achieved by first numerically estimating the derivative on the left-hand side of (11) using the measured intensity at two (or more) planes, e.g.,  $I(z_0)$  and  $I(z_0 + dz)$ , for a small  $dz$ . Then, after plugging in  $I(z_0)$  into the right-hand side of (11), a variety of methods can be applied to solve for  $\phi$  using appropriate

solve (S4). One class of such methods consists of greedy algorithms such as orthogonal matching pursuit [108]. Another popular method is based on convex relaxation of the  $\ell_0$  norm to an  $\ell_1$  norm [109], which yields the convex problem

$$\min_{\mathbf{x}} \|\mathbf{x}\|_1 \quad \text{s.t. } \mathbf{y} = \mathbf{Ax}. \quad (\text{S5})$$

In fact, under the condition (S2), it has been shown [107] that the solution to (S5) is equal to that of (S4).

Another important criterion to evaluate the recovery ability in sparse linear problems of the form (S1) is the restricted isometry property (RIP) [110] of  $\mathbf{A}$ . For an  $M \times N$  matrix  $\mathbf{A}$  (with  $M < N$ ), define the restricted isometry constant  $\delta_k$  as the smallest value such that for every submatrix  $\mathbf{A}_k$  composed of  $k$  columns of  $\mathbf{A}$

$$(1 - \delta_k) \|\mathbf{x}\|_2^2 \leq \|\mathbf{A}_k \mathbf{x}\|_2^2 \leq (1 + \delta_k) \|\mathbf{x}\|_2^2, \quad \forall \mathbf{x} \in \mathbb{R}^k. \quad (\text{S6})$$

The RIP is therefore a measure of whether  $\mathbf{A}$  preserves the energy of any  $k$ -sparse signal—which is the case if  $\delta_k$  is small. In the context of sparse recovery, it is used to prove uniqueness and noise-robustness results. For example, if  $\mathbf{A}$  is such that  $\delta_{2k} < \sqrt{2} - 1$ , then solving (S5) will yield the unique sparse solution to (S1). In practice, it is combinatorially difficult to calculate the RIP of a given matrix. However, certain random matrices can be shown to have good RIP with high probability. For example, an  $M \times N$  independent and identically distributed Gaussian matrix obeys the  $k$ -RIP with high probability, for  $M \sim O(k \log(N/k))$  [105]. This is one of the reasons that random matrices are favorable for sparse sensing.

boundary conditions and further assumptions (a common one is that  $I$  is constant in  $x, y$ , so that  $\nabla I = 0$  inside some boundary) [81]–[83], [99], [100].

The TIE approach requires acquisition of several images at different (and close) planes. It is relatively simple to implement when applicable and can produce phase measurements when the coherence of the light is not sufficient for interferometric measurements [101]. However, the necessity of multiple closely spaced imaging planes can naturally pose a limitation on possible applications, such as applications requiring a fast acquisition time or a high SNR. This is because multiple imaging planes require the use of beam splitters, which leads to signal loss. Some tradeoffs between different parameters in the TIE approach, e.g., the amount of defocus ( $dz$ ) versus recovery accuracy, are discussed in [102].

### SPARSITY-BASED ALGORITHMS

A specific kind of prior knowledge that can be incorporated into the phase-retrieval problem to help regularize it is the fact that the sought real-space object is sparse in some known representation (see “Sparse Linear Problems”). This means that the object  $x$  can be written as

$$x = \Psi\alpha \quad (12)$$

with  $\Psi$  being a representation matrix (the sparsity basis), and  $\alpha$  being a sparse vector, i.e., a vector containing a small number of nonzero coefficients. The simplest example is when the object is composed of a small number of point sources, in which case  $\Psi$  is the identity matrix. Equipped with such prior knowledge, one can hope to improve the performance of phase-retrieval algorithms by limiting the search for the true vector to the set of sparse vectors. There are several different ways that sparsity can be incorporated, which are described in this section.

### ALTERNATING PROJECTIONS WITH SPARSITY PRIOR

The Fienup algorithm described in the section “Alternating Projections” allows, in principle, for the incorporation of various types of general knowledge about the object, including sparsity [41], [103]. Sparsity was shown to be a useful prior in phase-retrieval algorithms already in 2004 [104] in the iterative charge-flipping algorithm, although it was not exploited directly (the electron density in [104] is assumed to have extended regions of zeros). More explicitly, the method in [103], for example, is based on the Fienup iterations, with the first three steps remaining unchanged.

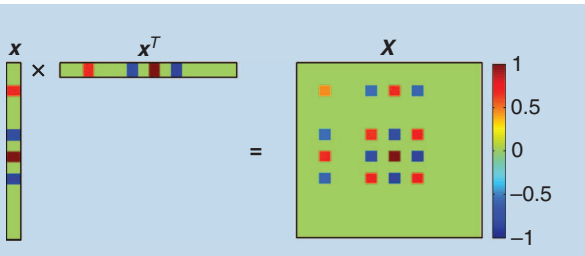


[FIG4] The sparse vector outer product yields a sparse matrix.

Step 4 is replaced by projection and thresholding. Assuming an invertible  $\Psi$  and a  $k$ -sparse vector  $\alpha$  such that  $x = \Psi\alpha$ :

4) Obtain  $z_{i+1}[n]$  by projecting  $z'_i[n]$  onto  $\Psi$ , thresholding, and projecting back.

- Calculate  $\alpha_i = \Psi^{-1}z'_i$ .
- Keep only the  $k$  largest elements of  $|\alpha_i|$ , setting the rest to zero.
- Set  $z_{i+1} = \Psi\alpha_i$ .

Similar to the GS iterations, the error here can be shown to be nonincreasing so that convergence to a local minimum is guaranteed [103].

Note, that while this method is suggested in [103] for an orthonormal basis  $\Psi$ , it can be easily modified to accommodate a noninvertible  $\Psi$ . This can be done by replacing the first two parts with finding a sparse solution  $a_i$  to  $z_i = \Psi\alpha_i$ , using any sparse solution approach [54].

### SDP-BASED METHODS WITH SPARSITY PRIOR

SDP methods can also be modified to account for prior knowledge of signal sparsity. The incorporation of sparsity may be performed in several different ways. The first work to suggest sparsity-based SDP phase retrieval came from the domain of optics and dealt with partially spatially incoherent illumination [46]. This work actually considered a theoretical problem of greater complexity, combining phase retrieval with subwavelength imaging. Experimental results on subwavelength CDI can be found in [45], where the sought signal is an optical image with subwavelength features, and the measured data correspond to the Fourier magnitude sampled by a camera at the focal plane of a microscope lens.

The method suggested in [46], dubbed *quadratic compressed sensing* (QCS), is based on adding sparsity constraints to the rank minimization problem (10). When  $x$  is sparse, the result of the outer product  $X = xx^*$  is a sparse matrix as well, as shown in Figure 4. Therefore, one strategy might be to minimize the  $l_1$  norm of the matrix  $X$ . Alternatively, it is possible to further exploit the structure of  $X$  by noticing that the number of rows in  $X$  with a nonzero norm is equal to the number of nonzero values in  $x$ . This means that the sparsity of  $x$  also implies a small number of nonzero rows in  $X$ . Consider the vector  $p$  containing the  $l_2$  norm of the rows of  $X$ , i.e.,  $p_j = (\sum_k |X_{jk}|^2)^{1/2}$  (note that the  $l_2$  norm can be replaced by any other norm). Since  $p$  should be sparse, one might try to impose a low  $l_1$  norm on  $p$ , in the spirit of  $l_1$  minimization for the sparse linear problem. This yields the constraint  $\|p\|_1 = \sum_j |p_j| = \sum_j (\sum_k |X_{jk}|^2)^{1/2} \leq \eta$ , corresponding exactly to a low mixed  $l_{1-2}$  norm constraint on  $X$  [111]. The problem to solve, as cast in [46], is therefore

$$\begin{aligned} & \min \text{rank}(X) \\ \text{s.t. } & |\text{Tr}(A_k X) - y_k| \leq \epsilon, \quad k = 1, \dots, M, \\ & X \succeq 0, \\ & \sum_j (\sum_k |X_{jk}|^2)^{1/2} \leq \eta, \end{aligned} \quad (13)$$

where  $\epsilon$  is a noise parameter and  $\eta$  is a sparsity parameter, enforcing row sparsity of  $X$ .

Since finding a rank-1 matrix  $\mathbf{X}$  satisfying the constraints is NP hard, the solution to (13) is approximated in [46] using the iterative log-det heuristic proposed in [97], with an additional thresholding step added at each iteration, to further induce signal sparsity. Once a low-rank matrix  $\hat{\mathbf{X}}$  that is consistent with the measurements and the sparse prior is found, the sought vector  $\mathbf{x}$  is estimated by taking the best rank-1 approximation of  $\hat{\mathbf{X}}$  using the singular value decomposition: Decomposing  $\hat{\mathbf{X}}$  into  $\hat{\mathbf{X}} = \mathbf{U}\mathbf{S}\mathbf{U}^*$ , the rank-1 approximation of  $\hat{\mathbf{X}}$  is taken as  $\hat{\mathbf{X}}_1 = \mathbf{S}_{11}\mathbf{U}_1\mathbf{U}_1^*$ , where  $\mathbf{S}_{11}$  represents the largest singular value, and  $\mathbf{U}_1$  is the corresponding column of  $\mathbf{U}$ .

Similar ideas that add sparse priors to SDP methods have been later suggested in [47], [57], and [112]. In [47], the rank minimization objective is relaxed to a convex trace minimization, with an additional  $\ell_1$  regularization term to induce sparsity. This formulation yields

$$\begin{aligned} \min \quad & \text{Tr}(\mathbf{X}) + \lambda \|\mathbf{X}\|_1 \\ \text{s.t.} \quad & |\text{Tr}(\mathbf{A}_k \mathbf{X}) - y_k| \leq \epsilon, \quad k = 1, \dots, M, \\ & \mathbf{X} \succeq 0. \end{aligned} \quad (14)$$

The solution of (14) is shown [47] to be unique in the noiseless case ( $\epsilon = 0$ ), under the following condition:  $\|\tilde{\mathbf{X}}\|_0 \leq (1/2)(1 + (1/\mu))$ , where  $\tilde{\mathbf{X}} = \bar{\mathbf{x}}\bar{\mathbf{x}}^*$ , with  $\bar{\mathbf{x}}$  being the true solution to (4). The mutual coherence  $\mu$  is defined by  $\mu = \max_{i,j}(|\langle \mathbf{B}_i, \mathbf{B}_j \rangle| / (\|\mathbf{B}_i\| \|\mathbf{B}_j\|))$ , with  $\mathbf{B}$  being the matrix satisfying  $\mathbf{y} = \mathbf{B}\mathbf{X}^S$ , where  $\mathbf{X}^S$  is the vector obtained from stacking the columns of  $\mathbf{X}$ . The same work also relates other recovery guarantees to the RIP criterion.

In [59] it is shown that for  $\mathbf{a}_i$  that are independent, zero-mean normal vectors, on the order of  $k^2 \log n$  measurements are sufficient to recover a  $k$ -sparse input from measurements of the form (4), using SDP relaxation. In [112], an algorithm is suggested to solve the sparse 1-D Fourier phase-retrieval problem based on a two-step process, with each step cast separately as an SDP problem: first, the support of  $\mathbf{x}$  is determined from its autocorrelation sequence, and then  $\mathbf{x}$  is found, given the support. This approach is shown experimentally to recover  $k$ -sparse signals from  $O(k^2)$  measurements.

### GREEDY METHODS WITH SPARSITY PRIOR

Since matrix-lifting algorithms involve a dimension increase, they are not ideally suited for large vectors, where the computational cost can become significant. In addition, they are generally not guaranteed to converge to a correct solution. An alternative is to use sparsity-based greedy methods [48], [51], [113]. One approach that is both fast and accurate is greedy sparse phase retrieval (GESPAR) [51]. GESPAR attempts to solve the least squares sparse quadratic problem (5). That is, it seeks a  $k$ -sparse vector  $\mathbf{x}$  consistent with the quadratic measurements  $\mathbf{y}$ . It is a fast, local search method, based on iteratively updating the signal support, seeking a vector that corresponds to the measurements under the current support constraint. A local search method is repeatedly invoked, beginning with an initial random support set. Then, at each iteration, a swap is performed between a support and an off-support index. Only two elements are changed in the swap (one in the support and one in the off-support), following the so-called two-opt

method [114]. Given the support of the signal, the phase-retrieval problem is then treated as a nonconvex optimization problem, approximated using the damped Gauss Newton method [115]. See Algorithm 2 for a general description.

---

#### Algorithm 2: GESPAR—Main steps.

---

**Input:**  $\mathbf{A}_i, y_i, \tau, \text{ITER}$ .

$\mathbf{A}_i \in \mathbb{R}^{N \times N}, i = 1, 2, \dots, M$  - symmetric matrices.

$y_i \in \mathbb{R}, i = 1, 2, \dots, M$ .

$\tau$ -threshold parameter.

**ITER** - Maximum allowed total number of swaps.

**Output:**  $\mathbf{x}$ -an optimal (or suboptimal) solution of (5).

---

**Initialization:** Set  $T = 0, j = 0$ .

1) Generate a random index set  $S_0 (|S_0| = s)$

2) Invoke the damped Gauss–Newton method with support  $S_0$  and obtain an output  $\mathbf{z}_0$ . Set  $\mathbf{x}_0 = \mathbf{U}_{S_0} \mathbf{z}_0$ , where  $\mathbf{U}_{S_0} \in \mathbb{R}^{N \times s}$  is the matrix consisting of the columns of the identity matrix  $\mathbf{I}_N$  corresponding to the index set  $S_0$

**General Step:** ( $j = 1, 2, \dots$ ):

3) Update support: Let  $p$  be the index from  $S_{j-1}$  corresponding to the component of  $\mathbf{x}_{j-1}$  with the smallest absolute value. Let  $q$  be the index from  $S_{j-1}^c$  corresponding to the component of  $\nabla f(\mathbf{x}_{j-1})$  with the highest absolute value, where  $\nabla f(\mathbf{x})$  is the gradient of the least-squares objective function from (5), i.e.,  $\nabla f(\mathbf{x}) = 4 \sum_i (\mathbf{x}^T \mathbf{A}_i \mathbf{x} - y_i) \mathbf{A}_i \mathbf{x}$ . Increase  $T$  by 1, and make a swap between the indices  $p$  and  $q$ , i.e., set  $\tilde{S}$  to be

$$\tilde{S} = (S_{j-1} \setminus \{p\}) \cup \{q\}.$$

4) Minimize with given support: Invoke the damped Gauss–Newton method [115] with input  $\tilde{S}$  and obtain an output  $\tilde{\mathbf{z}}$ . Set  $\tilde{\mathbf{x}} = \mathbf{U}_{\tilde{S}} \tilde{\mathbf{z}}$ , where  $\mathbf{U}_{\tilde{S}} \in \mathbb{R}^{N \times s}$  is the matrix consisting of the columns of the identity matrix  $\mathbf{I}_N$  corresponding to the index set  $S$ . If  $f(\tilde{\mathbf{x}}) < f(\mathbf{x}_{j-1})$ , then set  $S_j = \tilde{S}$ ,  $\mathbf{x}_j = \tilde{\mathbf{x}}$ , and go to Step 3. If none of the swaps resulted with a better objective function value, go to Step 1.

Until  $f(\mathbf{x}) < \tau$  or  $T > \text{ITER}$ .

The output is the solution  $\mathbf{x}$  that yields the minimum value for the least-squares objective.

---

GESPAR has been shown to yield fast and accurate recovery results (see “Sparse Phase-Retrieval Algorithms—A Comparison” and Figure S2) and has been used in several phase-retrieval optics applications, including CDI of 1-D objects [116], efficient CDI of sparsely temporally varying objects [52], and phase retrieval via waveguide arrays [53]. A similar approach has been applied to treat the combined phase-retrieval and subwavelength imaging problem [45] (see the section “Subwavelength CDI Using Sparsity”).

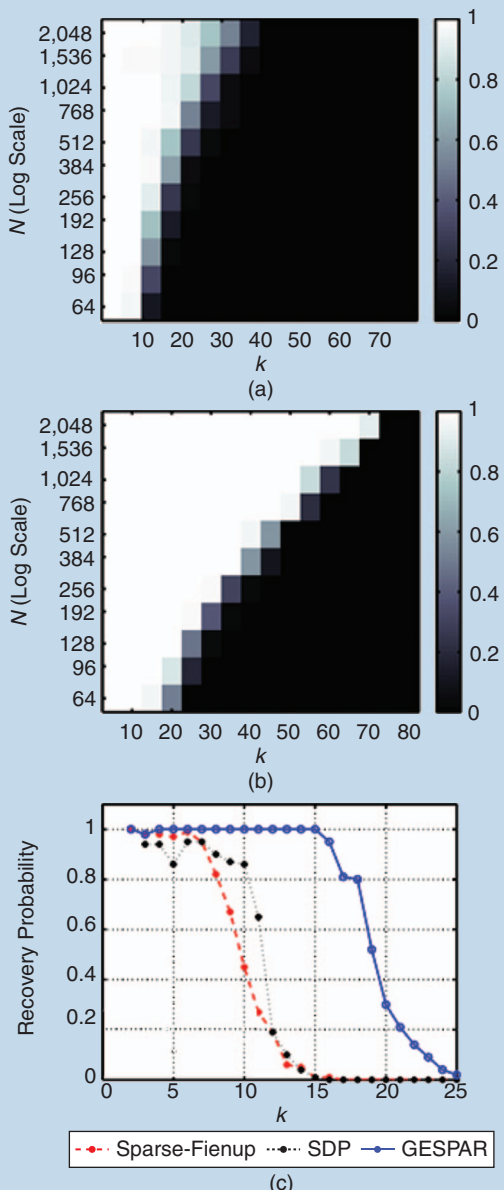
### APPLICATIONS IN LENSLESS IMAGING

In this section, we present several CDI applications with connection to the phase-retrieval algorithms described previously. The

## SPARSE PHASE-RETRIEVAL ALGORITHMS—A COMPARISON

We simulate sparse-Fienup [103] and GESPAR [51] for various values of  $N \in [64, 2,048]$ , and  $M = 2N$ . The recovery probability versus sparsity  $k$  for different vector lengths is shown in Figure S2(a) and (b). In both cases, the recovery probability increases with  $N$ , while GESPAR clearly outperforms the alternating iteration method.

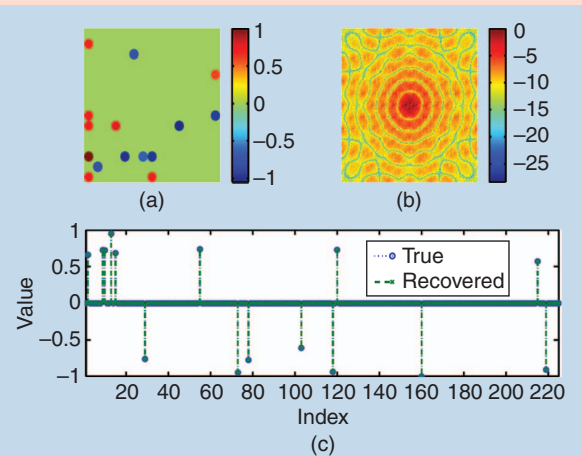
We then simulate the recovery success rate of three sparsity-based phase-retrieval algorithms. We choose  $\mathbf{x}$  as a



**[FIGS2]** A comparison of sparsity-based phase-retrieval algorithms. (a) The sparse-Fienup recovery probability versus sparsity  $k$ , for various signal length  $N$ , and with  $M = 2N$ . (b) GESPAR recovery probability versus sparsity  $k$  for various signal length  $N$ , and with  $M = 2N$ . (c) The recovery probability for three algorithms: sparse-Fienup, SDP, and GESPAR for  $N = 64$  and  $M = 128$  [51].

random vector of length  $N = 64$ . The vector contains uniformly distributed values in the range  $[-4, -3] \cup [3, 4]$  in  $k$  randomly chosen elements. The  $M = 128$  point DFT of the signal is calculated, and its magnitude-square is taken as  $\mathbf{y}$ , the vector of measurements. To recover the unknown vector  $\mathbf{x}$ , three methods are used: a greedy method (GESPAR [51]), an SDP-based method [112, Algorithm 2], and an iterative Fienup algorithm with a sparsity constraint [103]. The sparse-Fienup algorithm is run using 100 random initial points, out of which the chosen solution is the one that best matches the measurements.  $\hat{\mathbf{x}}$  is selected as the  $s$ -sparse output of the sparse-Fienup algorithm with the minimal cost  $f(\mathbf{x}) = \sum_{i=1}^N (|\mathbf{F}_i \mathbf{x}|^2 - y_i)^2$  out of the 100 runs. The probability of successful recovery is plotted in Figure 6(c) for different sparsity levels  $k$ . The success probability is defined as the ratio of correctly recovered signals  $\mathbf{x}$  out of 100 simulations. In each simulation, both the support and the signal values are randomly selected. The three algorithms (GESPAR, SDP, and sparse-Fienup) are compared. The results clearly show that GESPAR outperforms the other methods in terms of probability of successful recovery—more than 90% successful recovery up to  $k = 15$ , versus  $k = 8$  and  $k = 7$  in the other two techniques. For more extensive comparisons, we refer the reader to [51].

A major advantage of greedy methods over other techniques (e.g., SDP based) is their low computational cost; GESPAR may be used to find a sparse solution to the 2-D Fourier phase retrieval—or phase retrieval of images. Figure S3 shows a recovery example of a sparse  $195 \times 195$ -pixel image comprised of  $s = 15$  circles at random locations and random values on a grid containing 225 points, recovered from its 38,025 2-D Fourier magnitude measurements using GESPAR. The dictionary used in this example contains 225 elements consisting of nonoverlapping circles located on a  $15 \times 15$ -point Cartesian grid, each with a 13-pixel diameter. The solution took 80 s. Solving the same problem using the sparse-Fienup algorithm did not yield a successful reconstruction, and using the SDP method is not practical because of the large matrix size.



**[FIGS3]** A 2-D Fourier phase-retrieval example. (a) A true  $195 \times 195$  sparse circle image ( $s = 15$  circles). (b) The measured 2-D Fourier magnitude (38,025 measurements, log scale). (c) The true and recovered coefficient vectors corresponding to circle amplitudes at each of the 225 grid points [51].

concept of phase retrieval in optical imaging arises from the attempt to recover images from experimental measurements. To this end, it is essential to emphasize that, compared to numerical simulations or signal processing of digital data, phase retrieval of experimentally obtained patterns has several additional challenges. First, the far-field

intensity distribution (Fourier magnitude) is corrupted by various types of noise, such as Poisson noise, detector readout noise, and unwanted parasitic scattering from the optics components in the system. Second, in single-shot experiments, the measured far-field intensity distribution is usually incomplete, including a missing center (i.e., the very low spatial frequency information cannot be directly recorded by a detector) [85]. Third, when the far-field intensity distribution is measured by a detector, each pixel integrates the total number of photons within the solid angle subtended by the pixel, which is not exactly equivalent to uniform sampling of the diffraction signal [117]. Additionally, many experiments are carried out using incoherent (but bright) sources. Spatial optical coherence [to distinguish from the term *coherence* in signal processing, as defined by (S3)] is achieved by propagating a long distance from the source, but often the experiment is constrained to be carried out with a partially incoherent beam [118].

All of these issues add complications to algorithmic phase retrieval. However, notwithstanding these challenges, successful

**SINCE MATRIX-LIFTING ALGORITHMS INVOLVE A DIMENSION INCREASE, THEY ARE NOT IDEALLY SUITED FOR LARGE VECTORS, WHERE THE COMPUTATIONAL COST CAN BECOME SIGNIFICANT.**

phase retrieval of experimental data in optical imaging has been widely achieved [3], [13], [16], [17], [23], [28], [80], [119], [120]. Next we show several examples.

#### **QUANTITATIVE COMPARISON OF ALTERNATING-PROJECTION ALGORITHMS**

Quantitative comparisons between the OSS, HIO, ER-HIO, and NR-HIO algorithms have been performed using both simulated and experimental data [12]. Figure 5 shows a noise-free oversampled diffraction pattern (Fourier magnitude squared) calculated from a simulated biological vesicle [Figure 5(c)]. High Poisson noise was then added to the diffraction intensity [Figure 5(b)]. Figure 5(d)–(g) shows the final reconstructions by HIO, ER-HIO, NR-HIO, and OSS, respectively. Visually, OSS produced the most faithful reconstruction among the four algorithms [see the insets of Figure 5(d)–(g)]. The recovery error was quantified using consistency with the measurements

$$E = \sum_n |z_r[n] - z_m[n]| / \sum_n |z_m[n]|, \quad (15)$$

where  $z_r[n]$  is the final reconstruction and  $z_m[n]$  is the model structure. The value for  $E$  of the HIO, ER-HIO, NR-HIO, and OSS reconstructions is 0.28, 0.24, 0.16, and 0.07, respectively.

Next, the four algorithms were compared using an experimental diffraction pattern measured from a *Schizosaccharomyces*

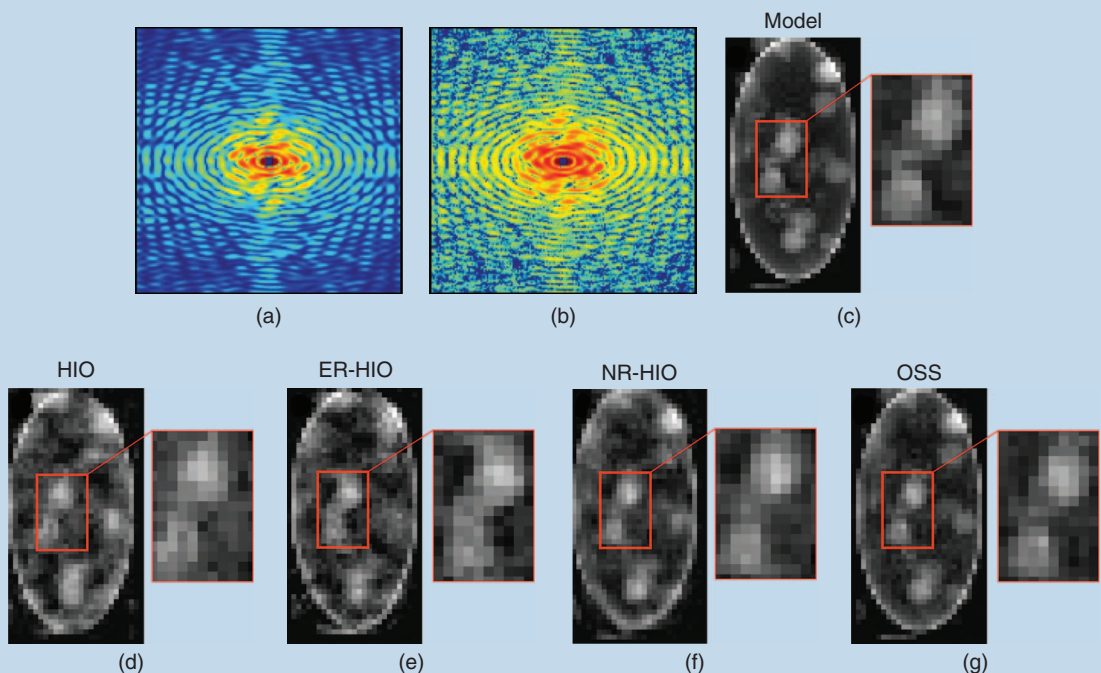


**[FIG5]** A quantitative comparison between the HIO, ER-HIO, NR-HIO, and OSS algorithms. (a) A noise-free oversampled diffraction pattern calculated from simulated biological vesicle. (b) The high Poisson noise added to the oversampled diffraction pattern. (c) The structure model of the biological vesicle and its fine features (inset). (b) The final reconstruction of the noisy diffraction pattern in (b) by (d) HIO, (e) ER-HIO, (f) NR-HIO, and (g) OSS [12].

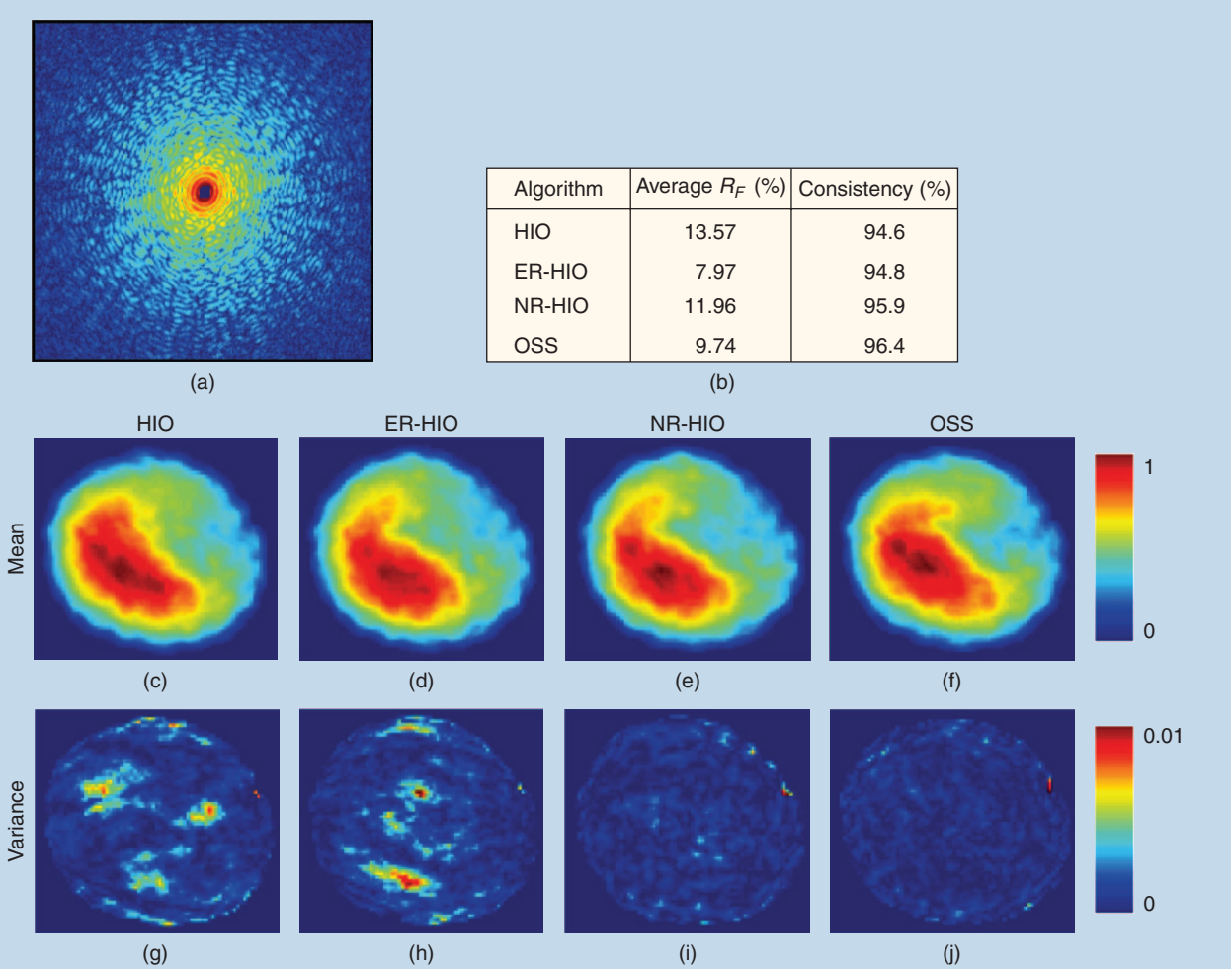


**[FIG6]** The phase retrieval of an experimental diffraction pattern from a biological sample. (a) An oversampled X-ray diffraction pattern measured from an *S. pombe* yeast spore cell. (b) The average  $R_F$  and the consistency of five independent trials of phase retrieval using four different algorithms. The average reconstruction of five independent trials using (c) HIO, (d) ER-HIO, (e) NR-HOP, and (f) OSS. The variance of five final images with (g) HIO, (h) ER-HIO, (i) NR-HOP, and (j) OSS [12].

*pombe* (*S. pombe*) yeast spore cell [12]. The experiment was conducted on an undulator beamline at a third-generation synchrotron radiation facility (Spring-8) in Japan. A coherent wave of 5 keV X-rays was incident on a fixed, unstained *S. pombe* yeast spore. An oversampled X-ray diffraction pattern was acquired by a CCD detector. Figure 6(a) shows the experimental diffraction pattern in which the centrosquare represents the missing low spatial resolution data [86]. By using a loose support, phase retrieval was performed on the measured data with the HIO, ER-HIO, NR-HIO, and OSS algorithms. For each algorithm, five independent trials were conducted, each consisting of 100 independent runs with different random initial phase sets. In each trial, the reconstruction with the smallest error metric  $R_F$  was chosen as a final image, where  $R_F$  is defined as

$$R_F = \sum_k \left| |Z_e[k]| - \zeta |Z_r[k]| \right| / \sum_k |Z_e[k]|. \quad (16)$$

Here,  $|Z_e[k]|$  is the measured Fourier magnitude,  $|Z_r[k]|$  is the recovered Fourier magnitude, and  $\zeta$  is a scaling factor.

For each algorithm, the mean and average of the five final images were used to quantify the reconstruction. Figure 6(c)–(j) shows the average and variance of five final images obtained by HIO, ER-HIO [75], NR-HIO [88], and OSS [12], respectively. The average  $R_F$  and the consistency of five independent trials are shown in Figure 6(b). Both visual inspection and quantitative results indicate that OSS produced the most consistent reconstructions among all four algorithms.

#### XFEL CDI

The majority of imaging experiments at XFEL sources use the method of CDI. The lensless nature of CDI is actually an advantage when dealing with extremely intense and destructive pulses, where one can only carry out a single pulse measurement with each object (say, a molecule) before the object

disintegrates. In such cases, often one cannot use any optical components at all, because any component, e.g., a lens, would be severely damaged by the extremely high flux of X-ray photons, and the damaged components will distort the measured data. CDI solves these problems: it works without the need for optical components. In this vein, CDI also facilitates reliable imaging of moving objects. Indeed, in many experiments, the objects move (flow) across the X-ray beam, for example, when the X-ray laser beam hits a focused aerosol beam or nanoparticles in a liquid jet. In such an experiment, the particle density is usually adjusted so that the X-ray laser pulse is more likely to hit a single particle than several. A particle is hit by chance by a pulse, but this is not known until the diffraction pattern is read out from the detector, which is done on every pulse. The stream of data is then analyzed and sorted to give the single-particle hits, which contain the meaningful measured data, while all other data are ignored.

There are two generic classes of these “single particle” CDI experiments: imaging of reproducible particles and imaging of unique particles. The first category includes particles such as viruses. Assuming that these particles are not aligned in the same direction, the collected data represent diffraction patterns of a common object, but in random orientations. If the orientations

can be determined, then the full 3-D Fourier magnitude of the object can be determined, which in turn could be phased to give a 3-D image. A proof of concept of this experiment was carried out by Loh et al. [121].

An example of the second class of flash diffractive imaging is imaging airborne soot particles in flight in an aerosol beam [28]. Several diffraction patterns of soot particles and clusters of polystyrene spheres as test objects are shown in Figure 7 along with the 2-D reconstructions of the objects. The experiments were carried out at the Linac Coherent Light Source using the Center for Free-Electron Laser Science-Advanced Study Group multipurpose instrument [122] at the atomic, molecular, and optical science beam line [123]. Pulses of about  $10^{12}$  photons of 1.0-nm wavelength were focused to an area of  $10 \mu\text{m}^2$ . The X-ray detectors (pnCCD panels) were placed to give a maximum full-period resolution of 13 nm

at their center edges.

In these experiments, the phase retrieval of the patterns was carried out using the RAAR [11] algorithm and shrinkwrap procedure [124], which determines and iteratively updates the support constraint used. The objects were such that it was possible to apply an additional constraint that the image is real valued. Strikingly, the X-ray coherent diffraction patterns have a very high contrast. The intensity minima are close to zero. This has an

## SPATIAL OPTICAL COHERENCE IS ACHIEVED BY PROPAGATING A LONG DISTANCE FROM THE SOURCE, BUT OFTEN THE EXPERIMENT IS CONSTRAINED TO BE CARRIED OUT WITH A PARTIALLY INCOHERENT BEAM.

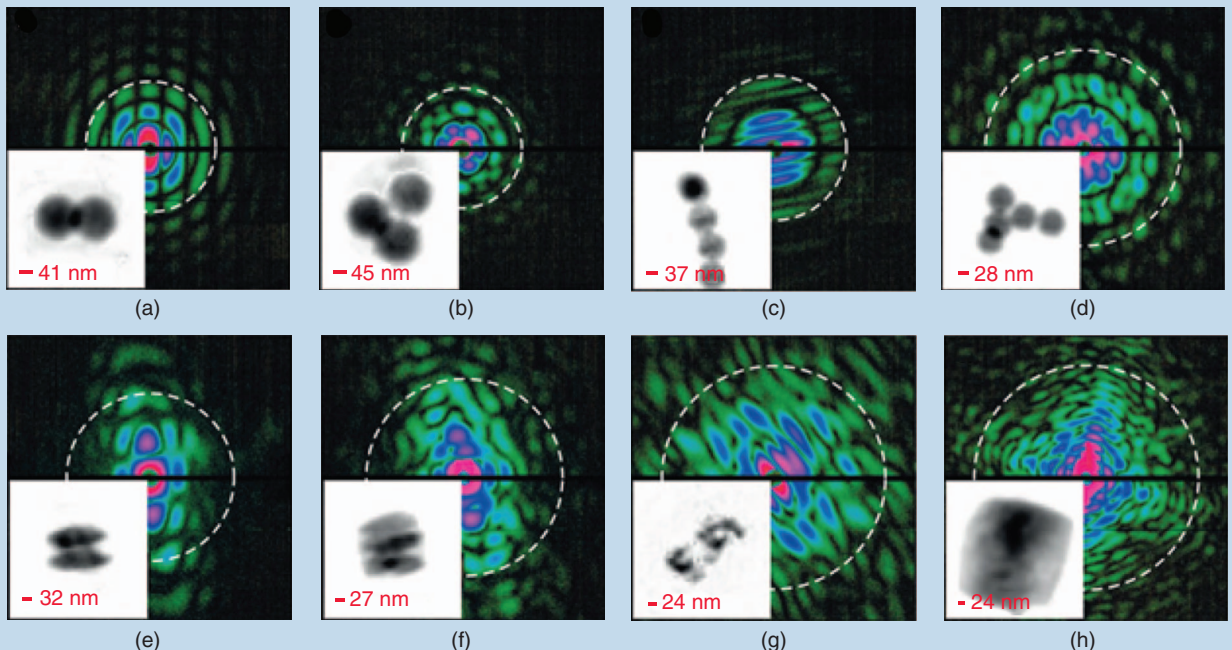


**[FIG7]** The diffraction patterns from single X-ray FEL pulses from particles in flight and reconstructed images: (a)–(d) clusters of polystyrene spheres with radii of (a) and (b) 70 nm, and (c) and (d) 44 nm; (e) and (f) ellipsoidal nanoparticles; (g) a soot particle; and (h) a salt-soot mixture [28].

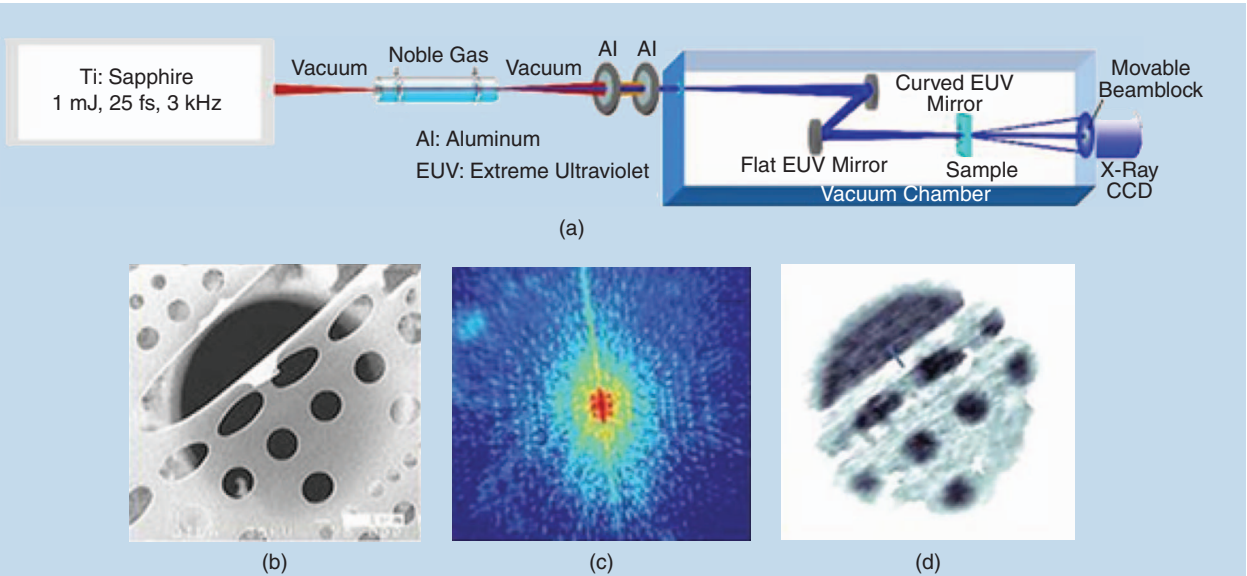


**[FIG8]** The first tabletop short-wavelength CDI. (a) The experimental setup. Coherent extreme UV radiation is generated through the process of high harmonic generation. A single harmonic order at wavelength 29 nm is selected and focused onto a sample by a pair of multilayer mirrors. The scattered light is detected by the X-ray CCD camera. (b) The original image, used to analyze the performance of the CDI process, obtained with a scanning electron microscope (SEM). The image shows a masked carbon film placed on a 15- $\mu\text{m}$  diameter pinhole. (c) The recorded multiframe diffraction pattern [corresponding to Fourier magnitude squared of the object shown in (b)]. (d) CDI reconstruction using the GHIO algorithm with 214-nm resolution [18].

enormous effect on the ability to recover the phase of these patterns reliably. This reliability is quantified in the phase-retrieval transfer function (PRTF) [125], which compares the magnitude of the complex-valued average of patterns phased with different starting guesses to the square root of the measured diffraction pattern. If, at a particular pixel of the diffraction pattern, the phases are consistently reconstructed, then the sum over  $N$  patterns will

give a magnitude  $N$  times higher than the measured magnitude, and so the PRTF will be unity. If the phases are random, then this sum will be close to zero. For patterns generated with XFELs, this function is often close to unity and is lower primarily in areas where the SNR is low.

Because the signal is limited, ultimately, so is the resolution; an estimate of the achieved resolution is given by the white dotted circle on each pattern in Figure 7. The reconstructed images are sums of ten independent reconstructions. These complex-valued sums have the property that their Fourier spectrum is effectively modulated by the PRTF and, hence, any artifact due to noise (or even due to forcibly truncating the data to a lower resolution) is unlikely to show up in the recovered image.

#### TABLETOP SHORT WAVELENGTH CDI

To date, most CDI experiments are carried out in third-generation synchrotron and XFELs. However, limited access and experimental time hinder the development and applications of CDI using these methods. Thus, over the past several years, CDI microscopes based on tabletop sources of coherent extreme ultraviolet and soft X-rays are also being developed [126]. Figure 8 shows the first tabletop CDI experiment with extreme UV wavelength.

Phase retrieval, i.e., obtaining Figure 8(d) from (c), is achieved using the GHIO algorithm [87]. In GHIO, the standard HIO is first run in parallel starting from several (16 in this case) random initial points, for a set number of iterations (2,000). This is generation zero of the algorithm. Then, the best output (in the sense of distance from the measurements) is selected to serve as the seed for the next generation. The inputs for the first generation are

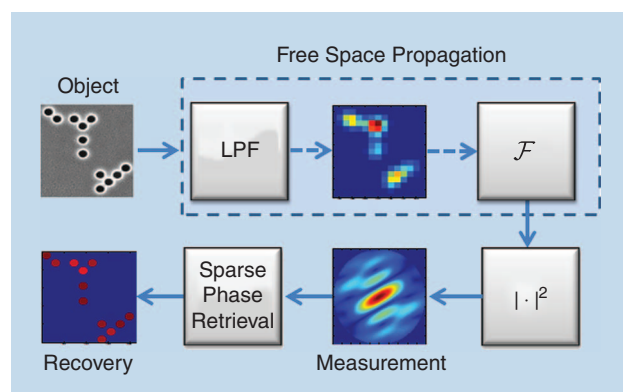


**[FIG9]** The sparsity-based subwavelength CDI. A 2-D object consisting of an arrangement of nanoholes (100 nm in diameter) is illuminated by a 532-nm laser, and the Fourier plane magnitude is measured. High spatial frequencies are lost during propagation, because the features (the circles as well as their separation) are smaller than  $\sim\lambda/2$ . Using an iterative greedy algorithm, and exploiting the prior knowledge that the object is sparse in a dictionary made of 100-nm circles, the phase is retrieved and the object is recovered from its low-pass-filtered Fourier magnitude [45].

obtained by multiplying the seed with each of the 16 images and taking the square root of the product. The same procedure is repeated for the next generations. The result in Figure 8(d) was obtained after the eighth generation, for which the 16 reconstructed images became consistent.

### SUBWAVELENGTH CDI USING SPARSITY

Prior knowledge of object sparsity can help regularize the phase-retrieval problem as well as compensate for loss of other kinds of information. Here, we consider a problem in which the high spatial frequencies are lost. As described before, when an object is illuminated by coherent light of wavelength  $\lambda$ , the far-field intensity pattern is proportional to the magnitude of the object's Fourier transform. In addition, features in the object that are smaller than  $\sim\lambda/2$  are smeared due to the diffraction limit. Consequently, the intensity measured in the far field corresponds to  $y \propto |\text{LF}_x|^2$ , where  $L$  represents a low-pass filter at cutoff frequency  $\nu_c = 1/\lambda$ ,  $F$  represents the Fourier transform, and  $|\cdot|^2$  stands for elementwise squared absolute value.

Figure 9 (adapted from [45]) shows the recovery of a sparse object containing subwavelength features (100-nm holes illuminated by a  $\lambda = 532$ -nm laser) from its experimentally measured low-pass-filtered Fourier magnitude. The prior knowledge used for recovery is that the object comprises a small number of 100-nm diameter circles on a grid, illuminated by a plane wave. The exact number, locations, and amplitudes of the circles are not known a priori. The recovery is performed using a greedy algorithm that iteratively updates the support of the object, finds a local minimum, and removes the weakest circle until convergence [45].

Another type of information loss in CDI, for which the prior knowledge of object sparsity can be helpful, is low SNR. In nondestructive X-ray CDI measurements, it is not uncommon for signal acquisition time to be on the order of tens of seconds [18], [20], [127] to achieve sufficiently high SNR. This poses a severe limitation on the temporal resolution attainable with such measurements, restricting the types of dynamical phenomena accessible by X-ray CDI. Exploiting sparsity in the change that an object undergoes between subsequent CDI frames has been recently suggested as a means to overcome high noise values and, consequently, significantly decrease acquisition time [52]. In other words, the fact that an object is sparsely varying can be used as prior information to effectively denoise sequential Fourier magnitude measurements. In [52], CDI of a sparsely varying object is formulated as a sparse quadratic optimization problem and solved using GESPAR [51]. Numerical simulations suggest a dramatic potential improvement in temporal resolution. In an example consisting of a  $51 \times 51$ -pixel object with five randomly varying pixels between frames, an improvement of two orders of magnitude in acquisition time is possible [52].

Finally, in [53], an experimental proof of concept is presented for an optical system in which discrete phase retrieval is performed using a small number of intensity measurements. The

system considered is a model multiple-input, multiple-output communication system: an array of coupled optical waveguides in which a small (sparse) number of input waveguides is excited. As the light propagates through the array, the energy couples into neighboring waveguides until, ultimately, at the output plane, the energy is distributed among many of the waveguides. The purpose is to recover the complex input field, i.e., which waveguides were excited, and at what amplitude and phase, given output intensities of only a subset of the waveguides. This problem is formulated as

a discrete phase-retrieval problem, and the loss of information, both of phase and of unmeasured waveguides, is compensated by a sparsity prior. The phase is then retrieved using GESPAR [51].

### KNOWLEDGE OF THE FOURIER PHASE SIGN HAS BEEN SHOWN TO YIELD UNIQUENESS WITH SOME RESTRICTIONS ON THE SIGNAL.

### OTHER PHYSICAL SETTINGS, BOTTLENECKS, AND VISION

This review article is focused on the simplest physical setting for phase retrieval in optical imaging (Figure 2), CDI: an unknown 2-D optical image is recovered algorithmically from a single measurement of its far-field intensity pattern, given a known image support (or other prior information). In terms of signal processing, this problem corresponds to recovering a 2-D object from measurements of its Fourier magnitude. However, the issue of phase retrieval in optical imaging and, in a more general sense, in optics is far broader and includes other physical settings that naturally translate into signal processing problems that are different than the standard phase-retrieval formulation. This section provides a short overview of those physical settings, defines the various problems in terms of signal processing, and provides some key references. We conclude with a discussion on the main challenges and bottlenecks of phase retrieval in optical imaging, followed by an outlook for the upcoming years and long-term vision.

### NON-FOURIER MEASUREMENTS

The simplest optical phase-retrieval problem assumes that the measured data corresponds to the Fourier magnitude. In optical settings, this means that the measurements are taken in the Fourier domain of the sought image, which physically means performing the measurements at a plane sufficiently far away from the image plane (the so-called far field or the Fraunhofer regime) or at the focal plane of an ideal lens [37]. In reality, however, the measurements can be taken at any plane between the image plane and the far field, which would yield intensity patterns that are very different than the Fourier magnitude of the signal. This of course implies that new (or revised) algorithms—beyond those described in previous sections—must be used, which naturally raises issues of conditions for uniqueness and convergence. At the same time, these measurements have some interesting advantages, which can be used wisely to improve the performance of phase retrieval. Let us begin by describing the relevant physical settings.

As stated earlier, the optical Fourier plane corresponds to a plane sufficiently far away from where the object (the sought signal) is

positioned. Far away here means asymptotically at infinite distance from the object plane or at the focal plane of a lens. However, the entire propagation-evolution of electromagnetic waves from any plane to any other plane is known: it is fully described by Maxwell's equations. As such, one can formulate the problem through a proper transfer function of the electromagnetic wave that is different than the Fourier transform.

In this context, the most well-studied case is the regime of Fresnel diffraction, where the transfer function is expressed in an integral form known as the *Fresnel integral* [37]. This regime occurs naturally at a range of distances away from the object plane, which naturally also includes the Fraunhofer regime where the transfer function reduces to a simple Fourier transform. Going beyond the Fresnel regime is also possible. This means that the (magnitude squared of the) electromagnetic wave will be measured at some arbitrary plane away from the object. A more general case arises by expressing the scalar transfer function of the light in a homogeneous medium, at any plane  $z$  as

$$T(k_x, k_y, z) = \exp[-iz\sqrt{k^2 - (k_x^2 + k_y^2)}]. \quad (17)$$

Here,  $k = \omega/c$ , with  $\omega$  being the frequency of the light,  $c$  being the speed of light in the medium, and  $k_x, k_y$  describe the transverse wavenumbers. The field at any arbitrary plane  $z$ ,  $E(x, y, z)$ , is then given by inverse Fourier transforming the spectral function at that plane  $F(k_x, k_y, z)$  [namely, the Fourier transform of  $E(x, y, z)$  with respect to  $x, y$ ], which is related to the spectrum at the initial plane by

$$F(k_x, k_y, z) = F(k_x, k_y, z=0)T(k_x, k_y, z).$$

With the transfer function (17), one can now formulate a new phase-retrieval problem, where the measurements are conducted at some arbitrary plane  $z$ , giving  $|E(x, y, z)|^2$ , and the sought signal is  $E(x, y, z=0)$ . This approach can be extended to include polarization effects, in which the transfer function is vectorial, thereby describing the propagation through Maxwell's equations with no approximation at all. The optical far field—where the measurement corresponds to the Fourier magnitude of the image at the initial plane (i.e., the measurement is proportional to  $|F(k_x, k_y, z)|^2$ )—is obtained for distances  $z$  larger than some minimum distance  $z_0$  that depends on the spectral extent of  $F(k_x, k_y, z=0)$ , and only within a region close enough to the  $z$ -axis in the measurement plane.

It is interesting to compare these more general phase-retrieval problems to the generic problem of recovering a signal from its Fourier magnitude. In terms of algorithmics, the generic problem is much simpler and was extensively studied throughout the years, whereas the general case is considerably more complex and was studied only sporadically. However, in terms of optics, the measurements in the general case can provide more information.

Namely, measurements of  $|E(x, y, z)|^2$  can be taken at multiple planes (multiple values of  $z$ ), and each measurement adds more information on the signal. In contrast, for the generic problem, once the measurements are taken in the optical far field, taking more measurements at further away distances does not add additional information because all of the far-field measurements correspond to the Fourier magnitude (to within some known scaling of coordinates in the measurement planes).

As such, performing phase retrieval of optical images in the most general (non-Fourier) case can be beneficial as it leads to multiple measurements, possibly relaxing the conditions on oversampling and/or the advance knowledge on the support in the image plane.

Historically, these ideas on non-Fourier measurements have been known to the optics community since the early days of optical phase retrieval [2]. They are currently being used in the context of improving the convergence of phase retrieval by taking non-Fourier measurements at several planes [14], [128]. Alternatively, one can take measurements at several different optical frequencies  $\omega$ , which would be expressed as different values of  $k = \omega/c$  in the general transfer function given before. In this multifrequency context, it is important that the frequencies are well separated, each having a narrow bandwidth, to conform the high degree of coherence required for CDI. These ideas are now being pursued by several groups [19], [118], [129]. Interestingly, the multifrequency idea also works in the continuous case of broad bandwidth pulses centered on a single frequency. In this case, the power spectrum of the pulse must be known in advance [118], [129], [130]. In a similar vein, recent work has demonstrated scanning CDI, where the beam is scanned through overlapping regions on the sample to allow imaging of extended objects, a method known as *ptychography* [80], [131]–[133].

More sophisticated physical settings also exist, where the medium within which the waves are propagating is not homogeneous in space. Famous examples are photonic crystals, wherein the refractive index varies periodically in space, in a known fashion, in one, two, or three dimensions. Obviously, in such settings, the transfer function for electromagnetic waves is fundamentally different from the transfer function in free space. The phase-retrieval problem in such systems, albeit less commonly known, is no less important. For example, photonic crystal fibers can in principle be used for imaging in endoscopy. The measurements in such systems correspond to the magnitude squared of the field at the measurement plane, which would be very different than the Fourier magnitude of the image. Still, once the transfer function is known, complicated as it may be, the phase-retrieval problem is well defined and can be solved with some modifications to the algorithms described earlier; see, e.g., the pioneering work on phase retrieval in a photonic crystal fiber [134], and very recently, work on sparsity-based phase retrieval and superresolution in optical waveguide arrays [53]. In addition to these, the concept of CDI has

also been extended to other schemes, such as Bragg CDI, suitable to periodic images to reconstruct the structure and strain of nanocrystals [135]–[138].

### PHASE RETRIEVAL COMBINING HOLOGRAPHIC METHODS

As explained earlier, optical settings always suffer from the inability of photodetectors to directly measure the phase of an electromagnetic wave at frequencies of terahertz and higher. A partial solution for this problem is provided through holography, which was invented by Denis Gabor in 1948 [139], who was awarded the Nobel Prize in Physics in 1971. Holography involves interfering an electromagnetic field carrying some image,  $E_{\text{image}}$ , with another electromagnetic field of the same frequency and a known structure, denoted as  $E_{\text{ref}}$ . Typically, the so-called reference wave,  $E_{\text{ref}}$ , has a very simple structure, for example, approximately a plane wave (wave of constant amplitude and phase). The detection system records  $|E_{\text{image}} + E_{\text{ref}}|^2$ . Originally, such holographic recording was done on a photographic plate that was made from a photosensitive material whose transmission, being sensitive to the intensity of the light, became proportional to the recorded pattern  $|E_{\text{image}} + E_{\text{ref}}|^2$ . Such a photographic plate is called a *hologram*, wherein the information contained in the image wave  $E_{\text{image}}$  is embedded in transmission function of the hologram. To see the recording, the wave of the known pattern,  $E_{\text{ref}}$ , is generated (which is possible because its structure is simple and fully known) and made to illuminate the hologram. The magnitude of the wave transmitted through the illuminated hologram is therefore proportional to  $|E_{\text{image}} + E_{\text{ref}}|^2 \cdot E_{\text{ref}}$ . One of the terms is  $|E_{\text{ref}}|^2 \cdot E_{\text{image}}$ . Since  $|E_{\text{ref}}|^2$  carries virtually no information, i.e., it is just a constant, this transmitted wave reconstructs the image times that constant. This is the principle of operation of holography. Over the years, it has been shown that it is almost always beneficial to record not the actual image but its Fourier spectrum; hence, the reconstructed information is the Fourier transform of the image, and the image itself is recovered either in the far field (as explained in the beginning of this article) or at the focal plane of a lens. This process is termed *Fourier holography* [140].

In the context of phase retrieval, holography is used to add information in the measurement scheme. Because in most cases the measurements used are Fourier magnitudes, which physically imply far-field measurements, the natural inclusion of holographic methods is through Fourier holography. For example, adding a tiny hole (a delta function) at a predetermined position in the sample, close to where the sought image resides, creates an additional wave in the far field with a tilted phase that arises from the displacement between the hole and the sought image. The far-field intensity, therefore, now corresponds to the absolute value squared of the sum of the Fourier transform of the sought image and the known wave. As such, it introduces additional prior knowledge that can be used for increased resolution of the algorithmic recovery or for

relaxing the constraints on the prior knowledge on the support. These ideas have been exploited successfully using X-rays and electrons by several groups [141]–[143].

### CHALLENGES

The current challenges can be briefly defined as higher resolution, the ability to recover more complex objects, improved robustness to noise, and real-time operation. The very reason phase retrieval in optical imaging has recently become so important is owing to the

**THE CURRENT CHALLENGES CAN BE BRIEFLY DEFINED AS HIGHER RESOLUTION, THE ABILITY TO RECOVER MORE COMPLEX OBJECTS, IMPROVED ROBUSTNESS TO NOISE, AND REAL-TIME OPERATION.**

vision to be able to one day directly image complex biological molecules, track their structural evolution as it evolves over time, and even view the dynamics of the electronic wave functions bonding atoms together. The reasoning is obvious: to understand biology at the molecular level and to decipher the secrets of how their atomic constituents bond together

and how they interact with other molecules. The current state of the art is far from those goals: imaging resolution is not yet at the atomic (subnanometer) level, and—at nanometric resolution—imaging cannot handle objects that are bounded by a support that is extremely large compared to the resolution. In terms of being able to perform real-time experiments, state-of-the-art measurements have demonstrated extremely short optical pulses: tens of attoseconds ( $10^{-18}$  s, on the order of the passage of a photon through a distance comparable to the size of an atom). Pioneering experiments have even started to probe the dynamics of electrons in molecules and tunneling processes on these timescales. But, as of today, none of these ultrafast methods was applied to imaging of even a simple molecule, let alone complex biological structures.

Clearly, the underlying physics and engineering pose great challenges to meet these goals. Generating coherent radiation in the hard X-ray regime is still a major obstacle, often requiring very large enterprises such as the X-ray sources at the SLAC National Accelerator Laboratory. These facilities around the world are continuously improving their photon flux at shorter wavelengths, thereby constantly improving imaging resolution. The fundamental limits on the coherent X-ray flux possible with current methods (such as synchrotrons, XFELs [55], [56], and the process of high harmonics generation [144]) are not even known. But the steady improvement does give hope for imaging at the atomic level in the near future. Taking the CDI techniques to the regime of attosecond science is an important challenge. These pulses are extremely short, and, hence, their bandwidth is huge. Therefore, the coherent diffraction pattern is a superposition of their multispectral contents, which requires new algorithmic methods. As described earlier, these issues are currently being explored by several groups. But the problem is fundamentally more complicated because the process of scattering of light by molecules at these short wavelengths and ultrashort timescales is not like passing light through a mask on which an image is imprinted. Rather, many issues related to light-matter interactions under these conditions are yet to be understood (e.g., tunneling ionization of atoms by laser pulses).

Finally, the long-term vision must include imaging the dynamics within complex biological systems at the atomic level and in real time. But such systems are extremely complex to handle, in terms of details on many spatial and temporal scales simultaneously, in terms of the statistical nature and huge redundancy in the physical processes taking place within such complexes simultaneously, and even in terms of the quantum mechanics governing the dynamics at those scales. This is where the signal processing community can make a large impact—by devising new and original methods for recovering the information from experimental measurements. Clearly, the algorithms will have to be tailored to the specific physical settings.

## AUTHORS

**Yoav Shechtman** (yoavsh@stanford.edu) received his B.Sc. degree in electrical engineering and physics in 2007 and his Ph.D. degree in physics in 2013 from the Technion–Israel Institute of Technology, Haifa, Israel. He is currently a postdoctoral scholar in the Department of Chemistry at Stanford University. His research interests include optical information processing, sparse information processing, single-molecule tracking, and fluorescence-based superresolution imaging. He is specifically interested in applying signal processing methods to practical biological/physical optical imaging problems. He has been awarded the Irwin and Joan Jacobs Excellence Scholarship for graduate studies and research, the Gutwirth Excellence Scholarship for graduate studies, and the Hershel Rich Innovation Award.

**Yonina C. Eldar** (yonina@ee.technion.ac.il) is a professor in the Department of Electrical Engineering at the Technion–Israel Institute of Technology, Haifa, Israel, and holds the Edwards Chair in Engineering. She has received numerous awards for excellence in research and teaching, including the Wolf Foundation Krill Prize for Excellence in Scientific Research, the Hershel Rich Innovation Award, the Michael Bruno Memorial Award from the Rothschild Foundation, the Weizmann Prize for Exact Sciences, the Muriel and David Jacknow Award for Excellence in Teaching, the IEEE Signal Processing Society Technical Achievement Award, and the IEEE/AESS Fred Nathanson Memorial Radar Award. She is the editor-in-chief of *Foundations and Trends in Signal Processing*. She is a Fellow of the IEEE. She is also a member of the Young Israel Academy of Science and the Israel Committee for Higher Education.

**Oren Cohen** (oren@tx.technion.ac.il) is an associate professor in the Department of Physics at the Technion–Israel Institute of Technology, Haifa, Israel. His research interests are mainly in extreme nonlinear optics, including high harmonic generation, laser filamentation, and spatiotemporal solitons, and also in structure-based superresolution in imaging, spectroscopy, and diagnostics of ultrashort laser pulses. He has received several awards including the Wolf Foundation Krill Prize for Excellence in Scientific Research and the Hershel Rich Innovation Award.

**Henry N. Chapman** (henry.chapman@desy.de) is the director of the Center for Free-Electron Laser Science at the Deutsches Elektronen-Synchrotron and the University of Hamburg in

Germany. He earned his Ph.D. degree in X-ray optics at the University of Melbourne, Australia. He has developed methods in coherent X-ray imaging, which began at Stony Brook University in New York. At Lawrence Livermore National Laboratory in California, he led a team to demonstrate that an intense X-ray free-electron laser pulse could outrun radiation damage. He continued this work to the atomic scale with the method of serial femtosecond X-ray crystallography, which promises to overcome current bottlenecks in protein structure determination. His current research is focused on developing this method and extending it to the smallest possible crystals, i.e., single molecules.

**Jianwei Miao** (miao@physics.ucla.edu) is a professor at the University of California, Los Angeles. He received an M.S. degree from the Chinese Academy of Science in 1994 and a Ph.D. degree from Stony Brook University in 1999. He conducted a seminal experiment on extending X-ray crystallography to allow structural determination of noncrystalline specimens in 1999. This method, known as *coherent diffractive imaging*, has been broadly implemented using synchrotron radiation, X-ray free-electron lasers, high harmonic generation, and electrons. In 2012, he demonstrated electron tomography at 2.4-Angstrom resolution, the highest resolution ever achieved in any general three-dimensional (3-D) imaging method. More recently, he applied electron tomography to observe nearly all the atoms in a platinum nanoparticle, and for the first time imaged the 3-D core structure of edge and screw dislocations at atomic resolution.

**Mordechai Segev** (msegev@tx.technion.ac.il) received his B.Sc. and Ph.D. degrees from the Technion–Israel Institute of Technology, Haifa, Israel, in 1985 and 1990. After three years of postdoctoral research at the California Institute of Technology, he joined Princeton University as an assistant professor in 1994, becoming an associate professor in 1997 and a professor in 1999. In 1998, he returned to Israel, resigning from Princeton in 2000. His research focuses on nonlinear optics, solitons, subwavelength imaging, and quantum electronics. He is a fellow of the Optical Society of America (OSA) and the American Physical Society (APS). He won numerous awards, among them the Quantum Electronics Prize of the European Physics Society, the Max Born Award of the OSA, and the Arthur Schawlow Prize of the APS. In 2011, he was elected to the Israel Academy of Sciences and Humanities, and in 2014 he won the Israel Prize in Physics. However, beyond his personal achievements, he takes pride in the success of his students and postdocs; 17 are now professors and others are leaders in industry.

## REFERENCES

- [1] D. Sayre. (1952, Nov.). Some implications of a theorem due to Shannon. *Acta Crystallogr.* [Online]. 5(6), pp. 843–843. Available: <http://scripts.iucr.org/cgi-bin/paper?a00763>
- [2] J. R. Fienup. (1978, July). Reconstruction of an object from the modulus of its Fourier transform. *Opt. Lett.* [Online]. 3(1), pp. 27–29. Available: <http://ol.osa.org/abstract.cfm?URI=ol-3-1-27>
- [3] J. Miao, P. Charalambous, J. Kirz and D. Sayre, “Extending the methodology of X-ray crystallography to allow imaging of micrometre-sized non-crystalline specimens,” *Nature*, vol. 400, no. 6742, pp. 342–344, 1999.

- [4] M. R. Howells, T. Beetz, H. N. Chapman, C. Cu, J. M. Holton, C. J. Jacobsen, J. Kirz, E. Lima, S. Marchesini, H. Miao, D. Sayre, D. A. Shapiro, J. C. H. Spence, and D. Starodub, (2009). An assessment of the resolution limitation due to radiation-damage in X-ray diffraction microscopy. *J. Electron Spectrosc. Relat. Phenom.* [Online]. 170(1–3), pp. 4–12. Available: <http://www.sciencedirect.com/science/article/pii/S0368204808001424>
- [5] J. C. Solem and G. C. Baldwin, "Microholography of living organisms," *Science*, vol. 218, no. 4569, pp. 229–235, 1982.
- [6] R. Neutze, R. Wouts, D. van der Spoel, E. Weckert, and J. Hajdu, "Potential for biomolecular imaging with femtosecond X-ray pulses," *Nature*, vol. 406, no. 6797, pp. 752–757, 2000.
- [7] J. Spence, U. Weierstall, and M. Howells, "Coherence and sampling requirements for diffractive imaging," *Ultramicroscopy*, vol. 101, no. 2, pp. 149–152, 2004.
- [8] V. Elser, "Solution of the crystallographic phase problem by iterated projections," *Acta Crystallogr. Sect. A*, vol. 59, no. 3, pp. 201–209, 2003.
- [9] S. Marchesini, "Invited article: A unified evaluation of iterative projection algorithms for phase retrieval," *Rev. Sci. Instrum.*, vol. 78, no. 1, pp. 011 301–011 301, 2007.
- [10] H. H. Bauschke, P. L. Combettes, and D. R. Luke, "Hybrid projection–reflection method for phase retrieval," *JOSA A*, vol. 20, no. 6, pp. 1025–1034, 2003.
- [11] D. R. Luke, "Relaxed averaged alternating reflections for diffraction imaging," *Inverse Probl.*, vol. 21, no. 1, p. 37, 2005.
- [12] J. A. Rodriguez, R. Xu, C.-C. Chen, Y. Zou, and J. Miao, "Oversampling smoothness: An effective algorithm for phase retrieval of noisy diffraction intensities," *J. Appl. Crystallogr.*, vol. 46, no. 2, pp. 312–318, 2013.
- [13] I. K. Robinson, I. A. Vartanyants, G. J. Williams, M. A. Pfeifer, and J. A. Pitney, "Reconstruction of the shapes of gold nanocrystals using coherent X-ray diffraction," *Phys. Rev. Lett.*, vol. 87, no. 19, p. 195505, 2001.
- [14] B. Abbey, K. A. Nugent, G. J. Williams, J. N. Clark, A. G. Peele, M. A. Pfeifer, M. D. Jonge, and I. McNulty, "Keyhole coherent diffractive imaging," *Nat. Phys.*, vol. 4, no. 5, pp. 394–398, 2008.
- [15] D. Nam, J. Park, M. Gallagher-Jones et al., "Imaging fully hydrated whole cells by coherent X-ray diffraction microscopy," *Phys. Rev. Lett.*, vol. 110, no. 9, pp. 098 103–103, 2013.
- [16] H. N. Chapman, A. Barty, M. J. Bogan, S. Boutet, M. Frank, S. P. Hau-Riege, S. Marchesini, B. W. Woods, S. C. Bajt, W. H. Benner, R. A. London, E. Plönjes, M. Kuhlmann, R. Treusch, S. Düsterer, T. Tschenkner, J. R. Schneider, E. Spiller, T. Möller, C. Bostedt, M. Hoener, D. A. Shapiro, K. O. Hodgson, D. van der Spoel, F. Burmeister, M. Bergh, C. Calamean, G. Huldt, M. M. Seibert, F. R. N. C. Maia, R. W. Lee, A. Szöke, N. Timneanu and J. Hajdu, "Femtosecond diffractive imaging with a soft-X-ray free-electron laser," *Nat. Phys.*, vol. 2, no. 12, pp. 839–843, 2006.
- [17] M. M. Seibert, T. Ekeberg, F. R. N. C. Maia, M. Svenda, J. Andreasson, O. Jönsson, D. Odić, B. Iwan, A. Rocker, D. Westphal, M. Hantke, D. P. DePonte, A. Barty, J. Schulz, L. Gumprecht, N. Coppola, A. Aquila, M. Liang, T. A. White, A. Martin, C. Caleman, S. Stern, C. Åbergel, V. Seltzer, J.-M. Claverie, C. Bostedt, J. D. Bozek, S. Boutet, A. A. Miahnahri, M. Messerschmidt, J. Krzywinski, G. Williams, K. O. Hodgson, M. J. Bogan, C. Y. Hampton, R. G. Sierra, D. Starodub, I. Andersson, S. Bajt, M. Barthelmess, J. C. H. Spence, P. Fromme, U. Weierstall, R. Kirian, M. Hunter, R. B. Doak, S. Marchesini, S. P. Hau-Riege, M. Frank, R. L. Shoeman, L. Lomb, S. W. Epp, R. Hartmann, D. Rolles, A. Rudenko, C. Schmidt, L. Foucar, N. Kimmel, P. Holl, B. Rudek, B. Erk, A. Hömke, C. Reich, D. Pietschner, G. Weidenspointner, L. Strüder, G. Hauser, H. Gorke, J. Ullrich, I. Schlichting, S. Herrmann, G. Schaller, F. Schopper, H. Soltau, K.-U. Kühnel, R. Andritschke, C.-D. Schröter, F. Krasniqui, M. Bott, S. Schorb, D. Rupp, M. Adolph, T. Gorkhov, H. Hirsemann, G. Potdevin, H. Graafsma, B. Nilsson, H. N. Chapman and J. Hajdu, (2011, Feb.). Single mimivirus particles intercepted and imaged with an X-ray laser, *Nature*. [Online]. 470(7332), pp. 78–81. Available: <http://dx.doi.org/10.1038/nature09748>.
- [18] R. L. Sandberg, A. Paul, D. A. Raymondson, S. Hädrich, D. M. Gaudiosi, J. Holtsnider, R. I. Tobey, O. Cohen, M. M. Murnane, H. C. Kapteyn, C. Song, J. Miao, Y. Liu, and F. Salmassi, (2007, Aug.). Lensless diffractive imaging using tabletop coherent high-harmonic soft-X-ray beams, *Phys. Rev. Lett.* [Online]. 99(9), p. 098103. Available: <http://link.aps.org/doi/10.1103/PhysRevLett.99.098103>
- [19] B. Chen, R. A. Dilanian, S. Teichmann, B. Abbey, A. G. Peele, G. J. Williams, P. Hannaford, L. V. Dao, H. M. Quiney, and K. A. Nugent, "Multiple wavelength diffractive imaging," *Phys. Rev. A*, vol. 79, no. 2, p. 23809, 2009.
- [20] M. D. Seaberg, D. E. Adams, E. L. Townsend, D. A. Raymondson, W. F. Schlotter, Y. Liu, C. S. Menoni, L. Rong, C.-C. Chen, J. Miao, H. C. Kapteyn, and M. M. Murnane, (2011, Nov.). Ultrahigh 22 nm resolution coherent diffractive imaging using a desktop 13 nm high harmonic source, *Opt. Express*. [Online]. 19(23), pp. 22 470–22 479. Available: <http://www.opticsexpress.org/abstract.cfm?URI=oe-19-23-22470>
- [21] R. L. Sandberg, C. Song, P. W. Wachulak, D. A. Raymondson, A. Paul, B. Amirbekian, E. Lee, A. E. Sakdinawat, C. La-O-Vorakiat, M. C. Marconi, C. S. Menoni, M. M. Murnane, J. J. Rocca, H. C. Kapteyn, and J. Miao, "High numerical aperture tabletop soft X-ray diffraction microscopy with 70-nm resolution," *Proc. Natl. Acad. Sci. U.S.A.*, vol. 105, no. 1, pp. 24–27, 2008.
- [22] J. Bertolotti, E. G. van Putten, C. Blum, A. Lagendijk, W. L. Vos, and A. P. Mosk, "Non-invasive imaging through opaque scattering layers," *Nature*, vol. 491, no. 7423, pp. 232–234, 2012.
- [23] J. M. Zuo, I. Vartanyants, M. Gao, R. Zhang, and L. A. Nagahara, "Atomic resolution imaging of a carbon nanotube from diffraction intensities," *Science*, vol. 300, no. 5624, pp. 1419–1421, 2003.
- [24] C. T. Putkunz, A. J. D'Alfonso, A. J. Morgan, M. Weyland, C. Dwyer, L. Bourgeois, J. Etheridge, A. Roberts, R. E. Scholten, K. A. Nugent, and L. J. Allen, "Atom-scale ptychographic electron diffractive imaging of boron nitride cones," *Phys. Rev. Lett.*, vol. 108, no. 7, p. 073901, 2012.
- [25] P. Thibault and V. Elser, "X-ray diffraction microscopy," *Annu. Rev. Condens. Matter Phys.*, vol. 1, no. 1, pp. 237–255, 2010.
- [26] K. A. Nugent, "Coherent methods in the X-ray sciences," *Adv. Phys.*, vol. 59, no. 1, pp. 1–99, 2010.
- [27] C. Song, H. Jiang, A. Mancuso, B. Amirbekian, L. Peng, R. Sun, S. S. Shah, Z. H. Zhou, T. Ishikawa, and J. Miao, "Quantitative imaging of single, unstained viruses with coherent x rays," *Phys. Rev. Lett.*, vol. 101, no. 15, p. 158101, 2008.
- [28] N. D. Loh, C. Y. Hampton, A. V. Martin, D. Starodub, R. G. Sierra, A. Barty, A. Aquila, J. Schulz, L. Lomb, J. Steinbrener, R. L. Shoeman, S. Kassemeyer, C. Bostedt, J. Bozek, S. W. Epp, B. Erk, R. Hartmann, D. Rolles, A. Rudenko, B. Rudek, L. Foucar, N. Kimmel, G. Weidenspointner, G. Hauser, P. Holl, E. Pedersoli, M. Liang, M. S. Hunter, L. Gumprecht, N. Coppola, C. Wunderer, H. Graafsma, F. R. N. C. Maia, T. Ekeberg, M. Hantke, H. Fleckenstein, H. Hirsemann, K. Nass, T. A. White, H. J. Tobias, G. R. Farquar, W. H. Benner, S. P. Hau-Riege, C. Reich, A. Hartmann, H. Soltau, S. Marchesini, S. Bajt, M. Barthelmess, P. Bucksbaum, K. O. Hodgson, L. Strüder, J. Ullrich, M. Frank, I. Schlichting, H. N. Chapman and M. J. Bogan, (2012, June). Fractal morphology, imaging and mass spectrometry of single aerosol particles in flight, *Nature*. [Online]. 486(7404), pp. 513–517. Available: <http://www.nature.com/nature/journal/v486/n7404/abs/nature11222.html>
- [29] R. A. Gonsalves, (1982). Phase retrieval and diversity in adaptive optics, *Opt. Eng.* [Online]. 21(5), pp. 215–229. Available: <http://dx.doi.org/10.1117/12.7972989>
- [30] J. E. Krist and C. J. Burrows, "Phase-retrieval analysis of pre-and post-repair hubble space telescope images," *Appl. Opt.*, vol. 34, no. 22, pp. 4951–4964, 1995.
- [31] D. R. Luke, J. V. Burke, and R. G. Lyon, "Optical wavefront reconstruction: Theory and numerical methods," *SIAM Rev.*, vol. 44, no. 2, pp. 169–224, 2002.
- [32] A. Labeyrie, "Attainment of diffraction limited resolution in large telescopes by Fourier analysing speckle patterns in star images," *Astron. Astrophys.*, vol. 6, no. 1, pp. 85–87, 1970.
- [33] J. C. Dainty and J. R. Fienup, "Phase retrieval and image reconstruction for astronomy," in *Image Recovery: Theory and Application*, H. Stark, Ed. San Diego, CA: Academic Press, 1987, pp. 231–275.
- [34] C. Lynds, S. Worden, and J. W. Harvey, "Digital image reconstruction applied to alpha orionis," *Astrophys. J.*, vol. 207, no. 1, pp. 174–180, July 1976.
- [35] A. W. Lohmann, G. Weigelt, and B. Wirnitzer, "Speckle masking in astronomy: Triple correlation theory and applications," *Appl. Opt.*, vol. 22, no. 24, pp. 4028–4037, 1983.
- [36] F. Roddier, *Adaptive Optics in Astronomy*. Cambridge, U.K.: Cambridge Univ. Press, 1999.
- [37] B. E. A. Saleh and M. C. Teich, *Fundamentals of Photonics*. Hoboken, NJ: Wiley, Mar. 2007.
- [38] E. J. Candès, T. Strohmer, and V. Voroninski, "PhaseLift: Exact and stable signal recovery from magnitude measurements via convex programming," *Commun. Pure Appl. Math.*, vol. 66, no. 8, pp. 1241–1274, 2013.
- [39] E. J. Candès, Y. C. Eldar, T. Strohmer, and V. Voroninski, "Phase retrieval via matrix completion," *SIAM J. Imag. Sci.*, vol. 6, no. 1, pp. 199–225, 2013.
- [40] R. Balan, P. Casazza, and D. Edidin, "On signal reconstruction without phase," *Appl. Comput. Harm. Anal.*, vol. 20, no. 3, pp. 345–356, 2006.
- [41] M. L. Moravec, J. K. Romberg, and R. G. Baraniuk, "Compressive phase retrieval," *Proc. SPIE*, vol. 6701, Wavelets XII, p. 670120, Sept. 2007.
- [42] A. Fannjiang, "Absolute uniqueness of phase retrieval with random illumination," *Inverse Probl.*, vol. 28, no. 7, p. 075008, 2012.
- [43] A. S. Bandeira, J. Cahill, D. G. Mixon, and A. A. Nelson, "Saving phase: Injectivity and stability for phase retrieval," *Appl. Computat. Harm. Anal.*, vol. 37, no. 1, pp. 106–125, 2014.
- [44] A. Beck and Y. C. Eldar, (2013). Sparsity constrained nonlinear optimization: Optimality conditions and algorithms, *SIAM J. Optim.* [Online]. 23(3), pp. 1480–1509. Available: <http://pubs.siam.org/doi/abs/10.1137/120869778>
- [45] A. Szameit, Y. Shechtman, E. Osherovich, E. Bullrich, P. Sidorenko, H. Dana, S. Steiner, E. B. Kley, S. Gazit, T. Cohen-Hyams, S. Shoham, M. Zibulevsky, I. Yavneh, Y. C. Eldar, O. Cohen, and M. Segev, (2012). Sparsity-based single-shot subwavelength coherent diffractive imaging, *Nat. Mater.* [Online]. 11(5), pp. 455–459. Available: <http://www.nature.com/nmat/journal/v11/n5/full/nmat3289.html>
- [46] Y. Shechtman, Y. C. Eldar, A. Szameit, and M. Segev, (2011, Aug.). Sparsity based sub-wavelength imaging with partially incoherent light via quadratic compressed sensing, *Opt. Express*. [Online]. 19(16), pp. 14 807–14 822. Available: <http://www.opticsexpress.org/abstract.cfm?URI=oe-19-16-14807>
- [47] H. Ohlsson, A. Y. Yang, R. Dong, and S. S. Sastry, "Compressive phase retrieval from squared output measurements via semidefinite programming," presented at the 16th IFAC Symposium on System Identification, SYSID 2012.

- [48] S. Bahmani, P. Boufounos, and B. Raj, "Greedy sparsity-constrained optimization," in *2011 Conf. Rec. Forty Fifth Asilomar Conf. Signals, Systems and Computers (ASILOMAR)*, 2011, pp. 1148–1152.
- [49] K. Jagannathan, S. Oymak, and B. Hassibi, "Recovery of sparse 1-d signals from the magnitudes of their fourier transform," in *Proc. 2012 IEEE Int. Symp. Information Theory (ISIT)*, 2012, pp. 1473–1477.
- [50] Y. C. Eldar and S. Mendelson. (2013). Phase retrieval: Stability and recovery guarantees. *Appl. Comput. Harm. Anal.* [Online]. Available: <http://www.sciencedirect.com/science/article/pii/S1063520313000717>
- [51] Y. Shechtman, A. Beck, and Y. C. Eldar, "GESPAR: Efficient phase retrieval of sparse signals," *IEEE Trans. Signal Processing*, vol. 62, no. 1–4, pp. 928–938, 2014.
- [52] Y. Shechtman, Y. C. Eldar, O. Cohen, and M. Segev. (2013, Mar.). Efficient coherent diffractive imaging for sparsely varying objects. *Opt. Express.* [Online]. 21(5), pp. 6327–6338. Available: <http://www.opticsexpress.org/abstract.cfm?URI=oe-21-5-6327>
- [53] Y. Shechtman, E. Small, Y. Lahini, M. Verbin, Y. C. Eldar, Y. Silberberg, and M. Segev. (2013, Oct.). Sparsity-based superresolution and phase-retrieval in waveguide arrays. *Opt. Express.* [Online]. 21(20), pp. 24 015–24 024. Available: <http://www.opticsexpress.org/abstract.cfm?URI=oe-21-20-24015>
- [54] Y. C. Eldar and G. Kutyniok, *Compressed Sensing: Theory and Applications*. Cambridge, U.K.: Cambridge Univ. Press, 2012.
- [55] P. Emma, R. Akre, J. Arthur, R. Bionta, C. Bostedt, J. Bozek, A. Brachmann, P. Bucksbaum, R. Coffee, F.-J. Decker, Y. Ding, D. Dowell, S. Edstrom, A. Fisher, J. Frisch, S. Gilovich, J. Hastings, G. Hays, Ph. Hering, Z. Huang, R. Iverson, H. Loos, M. Messerschmidt, A. Miahnahri, S. Moeller, H.-D. Nuhn, G. Pile, D. Ratner, J. Rzepiela, D. Schultz, T. Smith, P. Stefan, H. Tompkins, J. Turner, J. Welch, W. White, J. Wu, G. Yocky and J. Galayda, "First lasing and operation of an Ångstrom-wavelength free-electron laser," *Nat. Photon.*, vol. 4, no. 9, pp. 641–647, 2010.
- [56] T. Ishikawa, H. Aoyagi, T. Asaka, Y. Asano, N. Azumi, T. Bizen, H. Ego, K. Fukami, T. Fukui, Y. Furukawa, S. Goto, H. Hanaki, T. Hara, T. Hasegawa, T. Hatsui, A. Higashia, T. Hiroto, N. Hosoda, M. Ishii, T. Inagaki, Y. Inubushi, T. Itoga, Y. Joti, M. Kago, T. Kameshima, H. Kimura, Y. Kirihara, A. Kiyoimichi, T. Kobayashi, C. Kondo, T. Kudo, H. Maesaka, X. M. Maréchal, T. Masuda, S. Matsubara, T. Matsumoto, T. Matsushita, S. Matsui, M. Nagasono, N. Nariyama, H. Ohashi, T. Ohata, T. Ohshima, S. Ono, Y. Otake, C. Saji, T. Sakurai, T. Sato, K. Sawada, T. Seike, K. Shirasawa, T. Sugimoto, S. Suzuki, S. Takahashi, H. Takebe, K. Takeshita, K. Tamasaki, H. Tanaka, R. Tanaka, T. Tanaka, T. Togashi, K. Togawa, A. Tokuhisa, H. Tomizawa, K. Tono, S. Wu, M. Yabashi, M. Yamaga, A. Yamashita, K. Yanagida, C. Zhang, T. Shintake, H. Kitamura, and N. Kumagai, "A compact X-ray free-electron laser emitting in the sub-angstrom region," *Nat. Photon.*, vol. 6, no. 8, pp. 540–544, 2012.
- [57] I. Waldspurger, A. d'Aspremont, and S. Mallat, "Phase recovery, maxcut and complex semidefinite programming," *Math. Program.*, Ser. A, pp. 1–35, Dec. 2013.
- [58] P. Netrapalli, P. Jain, and S. Sanghavi, "Phase retrieval using alternating minimization," *Adv. Neural Inform. Process. Syst.*, pp. 2796–2804, 2013.
- [59] X. Li and V. Voroninski, "Sparse signal recovery from quadratic measurements via convex programming," *SIAM J. Math. Anal.*, vol. 45, no. 5, pp. 3019–3033, 2013.
- [60] G. David, F. Krahmer, and R. Kueng, "A partial derandomization of Phase Lift using spherical designs," arXiv preprint arXiv:1310.2267 (2013).
- [61] A. V. Oppenheim and J. S. Lim, "The importance of phase in signals," *Proc. IEEE*, vol. 69, no. 5, pp. 529–541, 1981.
- [62] E. Hofstetter, "Construction of time-limited functions with specified auto-correlation functions," *IEEE Trans. Inform. Theory*, vol. 10, no. 2, pp. 119–126, 1964.
- [63] Y. M. Bruck and L. Sodin, "On the ambiguity of the image reconstruction problem," *Opt. Commun.*, vol. 30, no. 3, pp. 304–308, 1979.
- [64] M. Hayes, "The reconstruction of a multidimensional sequence from the phase or magnitude of its Fourier transform," *IEEE Trans. Acoust., Speech Signal Processing*, vol. 30, no. 2, pp. 140–154, 1982.
- [65] R. H. T. Bates, "Fourier phase problems are uniquely solvable in more than one dimension. I: Underlying theory," *Optik*, vol. 61, no. 3, pp. 247–262, 1982.
- [66] J. Miao, D. Sayre, and H. Chapman, "Phase retrieval from the magnitude of the Fourier transforms of nonperiodic objects," *JOSAA*, vol. 15, no. 6, pp. 1662–1669, 1998.
- [67] P. L. Van Hove, M. H. Hayes, J. S. Lim, and A. V. Oppenheim, "Signal reconstruction from signed fourier transform magnitude," *IEEE Trans. Acoust., Speech Signal Processing*, vol. 31, no. 5, pp. 1286–1293, 1983.
- [68] M. Elad, *Sparse and Redundant Representations: From Theory to Applications in Signal and Image Processing*. New York: Springer-Verlag, 2010.
- [69] J. Ranieri, A. Chebira, Y. M. Lu, and M. Vetterli, "Phase retrieval for sparse signals: Uniqueness conditions," Preprints, arXiv:1308.3058 (2013).
- [70] H. Ohlsson and Y. C. Eldar, "On conditions for uniqueness in sparse phase retrieval," Preprints, arXiv:1308.5447 (2013).
- [71] K. Jagannathan, S. Oymak, and B. Hassibi. (2013, Nov.). Sparse phase retrieval: Uniqueness guarantees and recovery algorithms. arXiv:1311.2745 [cs, math]. [Online]. Available: <http://arxiv.org/abs/1311.2745>
- [72] E. Osherovich, M. Zibulevsky, and I. Yavneh, "Approximate Fourier phase information in the phase retrieval problem: What it gives and how to use it," *JOSAA*, vol. 28, no. 10, pp. 2124–2131, 2011.
- [73] E. Candes, X. Li, and M. Soltanolkotabi, "Phase retrieval from masked Fourier transforms," Preprints, arXiv:1310.3240 (2013).
- [74] R. Gerchberg and W. Saxton, "A practical algorithm for the determination of phase from image and diffraction plane pictures," *Optik*, vol. 35, p. 237, 1972.
- [75] J. Fienup, "Phase retrieval algorithms: A comparison," *Appl. Opt.*, vol. 21, no. 15, pp. 2758–2769, 1982.
- [76] D. Misell, "An examination of an iterative method for the solution of the phase problem in optics and electron optics: I. test calculations," *J. Phys. D: Appl. Phys.*, vol. 6, no. 18, p. 2200, 1973.
- [77] A. Huiser and H. Ferwerda, "The problem of phase retrieval in light and electron microscopy of strong objects: II. On the uniqueness and stability of object reconstruction procedures using two defocused images," *J. Mod. Opt.*, vol. 23, no. 6, pp. 445–456, 1976.
- [78] W. Hoppe and G. Strube, "Beugung in inhomogenen primärstrahlenwellenfeld. II. lichtoptische analogieversuche zur phasenmessung von gitterinterferenzen," *Acta Crystallogr. Sect. A*, vol. 25, no. 4, pp. 502–507, 1969.
- [79] J. Rodenburg, "Ptychography and related diffractive imaging methods," *Adv. Imag. Electron Phys.*, vol. 150, pp. 87–184, 2008.
- [80] M. Dierolf, A. Menzel, P. Thibault, P. Schneider, C. M. Kewish, R. Wepf, O. Bunk and F. Pfeiffer, "Ptychographic X-ray computed tomography at the nanoscale," *Nature*, vol. 467, no. 7314, pp. 436–439, 2010.
- [81] M. Reed Teague, "Deterministic phase retrieval: A green's function solution," *JOSA*, vol. 73, no. 11, pp. 1434–1441, 1983.
- [82] N. Streibl. (1984). Phase imaging by the transport equation of intensity. *Opt. Commun.* [Online]. 49(1), pp. 6–10. Available: <http://www.sciencedirect.com/science/article/pii/0030401884900798>
- [83] T. E. Gureyev and K. A. Nugent, "Phase retrieval with the transport-of-intensity equation. ii. orthogonal series solution for nonuniform illumination," *JOSAA*, vol. 13, no. 8, pp. 1670–1682, 1996.
- [84] J. R. Fienup. (1987, Jan.). Reconstruction of a complex-valued object from the modulus of its Fourier transform using a support constraint. *J. Opt. Soc. Am. A* [Online]. 4(1), pp. 118–123. Available: <http://josaa.osa.org/abstract.cfm?URI=josaa-4-1-118>
- [85] J. Miao, Y. Nishino, Y. Kohmura, B. Johnson, C. Song, S. H. Risbud, and T. Ishikawa, "Quantitative image reconstruction of GaN quantum dots from oversampled diffraction intensities alone," *Phys. Rev. Lett.*, vol. 95, no. 8, p. 085503, 2005.
- [86] H. Jiang, C. Song, C.-C. Chen, R. Xu, K. S. Raines, B. P. Fahimian, C.-H. Lu, T.-K. Lee, A. Nakashima, J. Urano, T. Ishikawa, F. Tamanoi, and J. Miao, "Quantitative 3D imaging of whole, unstained cells by using X-ray diffraction microscopy," *Proc. Natl. Acad. Sci. U.S.A.*, vol. 107, no. 25, pp. 11 234–11 239, 2010.
- [87] C.-C. Chen, J. Miao, C. W. Wang, and T. K. Lee, "Application of optimization technique to noncrystalline X-ray diffraction microscopy: Guided hybrid input-output method," *Phys. Rev., Ser. B*, vol. 76, no. 6, p. 064113, 2007.
- [88] A. V. Martin, F. Wang, N. D. Loh, T. Ekeberg, F. R. N. C. Maia, M. Hantke, G. van der Schot, C. Y. Hampton, R. G. Sierra, A. Aquila, S. Bajt, M. Barthelmes, C. Bostedt, J. D. Bozek, N. Coppola, S. W. Epp, B. Erk, H. Fleckenstein, L. Foucar, M. Frank, H. Graafsmo, L. Gumprecht, A. Hartmann, R. Hartmann, G. Hauser, H. Hirsemann, P. Holl, S. Kassemeyer, N. Kimmel, M. Liang, L. Lomb, S. Marchesini, K. Nass, E. Pedersoli, C. Reich, D. Rolles, B. Rudek, A. Rudenko, J. Schulz, R. L. Shoeman, H. Soltau, D. Starodub, J. Steinbrener, F. Stellato, L. Strüder, J. Ulrich, G. Weidenspointner, T. A. White, C. B. Wunderer, A. Barty, I. Schlichting, M. J. Bogan, and H. N. Chapman. (2012, July). "Noise-robust coherent diffractive imaging with a single diffraction pattern," *Opt. Express.* [Online]. 2015, pp. 16,650–16,661. Available: <http://www.opticsexpress.org/abstract.cfm?URI=oe-20-15-16650>
- [89] D. C. Youla and H. Webb, "Image restoration by the method of convex projections: Part 1 - theory," *IEEE Trans. Medical Imaging*, vol. 1, no. 2, pp. 81–94, 1982.
- [90] A. Levi and H. Stark, "Signal restoration from phase by projections onto convex sets," *JOSA*, vol. 73, no. 6, pp. 810–822, 1983.
- [91] A. Levi and H. Stark, "Image restoration by the method of generalized projections with application to restoration from magnitude," *JOSAA*, vol. 1, no. 9, pp. 932–943, 1984.
- [92] H. Bauschke, P. Combettes, and D. Luke, "Phase retrieval, error reduction algorithm, and Fienup variants: A view from convex optimization," *JOSAA*, vol. 19, no. 7, pp. 1334–1345, 2002.
- [93] E. Chouzenoux, J.-C. Pesquet, and A. Repetti, "A block coordinate variable metric forward-backward algorithm," *Optim. Online*, 2013. [Online]. Available: <https://hal.archives-ouvertes.fr/hal-00945918/>
- [94] J. Douglas and H. Rachford, "On the numerical solution of heat conduction problems in two and three space variables," *Trans. Amer. Math. Soc.*, vol. 82, no. 2, pp. 421–439, 1956.
- [95] P.-L. Lions and B. Mercier, "Splitting algorithms for the sum of two nonlinear operators," *SIAM J. Numer. Anal.*, vol. 16, no. 6, pp. 964–979, 1979.
- [96] L. Vandenberghe and S. Boyd, "Semidefinite programming," *SIAM Rev.*, vol. 38, no. 1, pp. 49–95, 1996.
- [97] M. Fazel, H. Hindi, and S. P. Boyd, "Log-det heuristic for matrix rank minimization with applications to Hankel and Euclidean distance matrices," in *Proc. 2003 IEEE American Control Conf.*, vol. 3, pp. 2156–2162.

- [98] M. X. Goemans and D. P. Williamson, "Improved approximation algorithms for maximum cut and satisfiability problems using semidefinite programming," *J. ACM*, vol. 42, no. 6, pp. 1115–1145, 1995.
- [99] F. Roddier, "Wavefront sensing and the irradiance transport equation," *Appl. Opt.*, vol. 29, no. 10, pp. 1402–1403, 1990.
- [100] L. Waller, L. Tian, and G. Barbastathis, "Transport of intensity phase-amplitude imaging with higher order intensity derivatives," *Opt. Express*, vol. 18, no. 12, pp. 12 552–12 561, 2010.
- [101] D. Paganin and K. A. Nugent, "Noninterferometric phase imaging with partially coherent light," *Phys. Rev. Lett.*, vol. 80, no. 12, p. 2586, 1998.
- [102] D. Paganin, A. Barty, P. McMahon et al., "Quantitative phase-amplitude microscopy. III. The effects of noise," *J. Microsc.*, vol. 214, no. 1, pp. 51–61, 2004.
- [103] S. Mukherjee and C. Seelamantula, "An iterative algorithm for phase retrieval with sparsity constraints: Application to frequency domain optical coherence tomography," in *Proc. 2012 IEEE Int. Conf. Acoustics, Speech, and Signal Processing (ICASSP)*, pp. 553–556.
- [104] G. Oszlányi and A. Suto, "Ab initio structure solution by charge flipping," *Acta Crystallogr., Sect. A*, vol. 60, no. 2, pp. 134–141, 2004.
- [105] E. Candes, J. Romberg, and T. Tao, "Robust uncertainty principles: Exact signal reconstruction from highly incomplete frequency information," *IEEE Trans. Inform. Theory*, vol. 52, no. 2, pp. 489–509, Feb. 2006.
- [106] D. Donoho, "Compressed sensing," *IEEE Trans. Inform. Theory*, vol. 52, no. 4, pp. 1289–1306, 2006.
- [107] D. L. Donoho and M. Elad, (2003, Mar.). Optimally sparse representation in general (nonorthogonal) dictionaries via l1 minimization. *Proc. Natl. Acad. Sci. U.S.A.* [Online]. 100(5), pp. 2197–2202. Available: <http://www.pnas.org/content/100/5/2197>
- [108] Y. C. Pati, R. Rezaifar, and P. Krishnaprasad, "Orthogonal matching pursuit: Recursive function approximation with applications to wavelet decomposition," in *1993 Conf. Rec. 27th Asilomar Conf. Signals, Systems and Computers*, IEEE, 1993, pp. 40–44.
- [109] S. S. Chen, D. L. Donoho, and M. A. Saunders, (1998, Jan.). Atomic decomposition by basis pursuit," *SIAM J. Sci. Comput.* [Online]. 20(1), pp. 33–61. Available: <http://pubs.siam.org/doi/abs/10.1137/S1064827596304010>
- [110] E. Candes and T. Tao, "Decoding by linear programming," *IEEE Trans. Inform. Theory*, vol. 51, no. 12, pp. 4203–4215, 2005.
- [111] M. F. Duarte and Y. C. Eldar, "Structured compressed sensing: From theory to applications," *IEEE Trans. Signal Processing*, vol. 59, no. 9, pp. 4053–4085, 2011.
- [112] K. Jagannathan, S. Oymak, and B. Hassibi, "Recovery of sparse 1-D signals from the magnitudes of their Fourier transform," in *2012 IEEE Int. Symp. Information Theory Proc. (ISIT)*, 2012, pp. 1473–1477.
- [113] A. Beck and Y. C. Eldar, (2012, Mar.). Sparsity constrained nonlinear optimization: Optimality conditions and algorithms. *arXiv:1203.4580*. [Online]. Available: <http://arxiv.org/abs/1203.4580>
- [114] C. H. Papadimitriou and K. Steiglitz, *Combinatorial Optimization: Algorithms and Complexity*. New York: Dover, 1998.
- [115] D. P. Bertsekas, "Nonlinear programming," 1999.
- [116] P. Sidorenko, A. Fleischer, Y. Shechtman, Y. C. Eldar, M. Segev, and O. Cohen, "Sparsity-based superresolution coherent diffractive imaging of (practically) 1D images using extreme UV radiation," in *Proc. CLEO: 2013*. Optical Society of America, 2013, p. QFIC.7
- [117] C. Song, D. Ramunno-Johnson, Y. Nishino, Y. Kohmura, T. Ishikawa, C.-C. Chen, T.-K. Lee, and J. Miao, "Phase retrieval from exactly oversampled diffraction intensity through deconvolution," *Phys. Rev. B*, vol. 75, no. 1, p. 012102, 2007.
- [118] L. Whitehead, G. J. Williams, H. M. Quiney, D. J. Vine, R. A. Dilanian, S. Flewett, K. A. Nugent, A. G. Peele, E. Balaur, and I. McNulty, "Diffractive imaging using partially coherent x rays," *Phys. Rev. Lett.*, vol. 103, no. 24, p. 243902, 2009.
- [119] G. J. Williams, M. A. Pfeifer, I. A. Vartanyants, and I. K. Robinson, "Three-dimensional imaging of microstructure in au nanocrystals," *Phys. Rev. Lett.*, vol. 90, no. 17, p. 175501, 2003.
- [120] C. Song, H. Jiang, A. Mancuso, B. Amirbekian, Li Peng, R. Sun, S. S. Shah, Z. H. Zhou, T. Ishikawa, and J. Miao, "Quantitative imaging of single, unstained viruses with coherent x rays," *Phys. Rev. Lett.*, vol. 101, no. 15, p. 158101, 2008.
- [121] N. D. Loh, M. J. Bogan, V. Elser, A. Barty, S. Boutet, S. Bajt, J. Hajdu, T. Ekeberg, F. R. N. C. Maia, J. Schulz, M. M. Seibert, B. Iwan, N. Timneanu, S. Marchesini, I. Schlichting, R. L. Shoeman, L. Lomb, M. Frank, M. Liang, and H. N. Chapman, "Cryptotomography: Reconstructing 3D Fourier intensities from randomly oriented single-shot diffraction patterns," *Phys. Rev. Lett.*, vol. 104, no. 22, p. 225501, 2010.
- [122] L. Strüder, S. Epp, D. Rolles, R. Hartmann, P. Holl, G. Lutz, H. Soltau, R. Eckart, C. Reich, K. Heinzinger, C. Thamm, A. Rudenko, F. Krasnigi, K.-U. Künnel, C. Bauer, C.-D. Schröter, R. Moshammer, S. Techert, D. Miessner, M. Porro, O. Häcker, N. Meidinger, N. Kimmel, R. Andritschke, F. Schopper, G. Weidenspointner, A. Ziegler, D. Pietschner, S. Herrmann, U. Pietsch, A. Walenta, W. Leitenberger, C. Bostedt, T. Möller, D. Rupp, M. Adolph H. Graafsma, H. Hirsemann, K. Gärtner, R. Richter, L. Foucar, R. L. Shoeman, I. Schlichting, and J. Ullrich, "Large-format, high-speed, X-ray PNCCDs combined with electron and ion imaging spectrometers in a multipurpose chamber for experiments at 4th generation light sources," *Nucl. Instrum. Meth. Phys. Res. Sect. A*, vol. 614, no. 3, pp. 483–496, 2010.
- [123] J. Bozek, "Amo instrumentation for the Icls X-ray fel," *Eur. Phys. J. Special Top.*, vol. 169, no. 1, pp. 129–132, 2009.
- [124] S. Marchesini, H. He, H. N. Chapman, S. P. Hau-Riege, A. Noy, M. R. Howells, U. Weierstall, and J. C. H. Spence, (2003, Oct.). X-ray image reconstruction from a diffraction pattern alone. *Phys. Rev. B* [Online]. vol. 68, p. 140101. Available: <http://link.aps.org/doi/10.1103/PhysRevB.68.140101>
- [125] H. N. Chapman, A. Barty, S. Marchesini, A. Noy, S. P. Hau-Riege, C. Cui, M. R. Howells, R. Rosen, H. He, J. C. H. Spence, U. Weierstall, T. Beetz, C. Jacobsen, and D. Shapiro, "High-resolution ab initio three-dimensional X-ray diffraction microscopy," *JOSA A*, vol. 23, no. 5, pp. 1179–1200, 2006.
- [126] R. L. Sandberg, Z. Huang, R. Xu, J. A. Rodriguez, and J. Miao, "Studies of materials at the nanometer scale using coherent X-ray diffraction imaging," *JOM*, vol. 65, no. 9, pp. 1208–1220, 2013.
- [127] L.-M. Stadler, C. Gutt, T. Autenrieth, O. Leupold, S. Rehbein, Y. Chushkin, and G. Grüber, (2008, June). Hard x ray holographic diffraction imaging. *Phys. Rev. Lett.* [Online]. 100(24), p. 245503. Available: <http://link.aps.org/doi/10.1103/PhysRevLett.100.245503>
- [128] G. J. Williams, H. M. Quiney, B. B. Dhal, C. Q. Tran, K. A. Nugent, A. G. Peele, D. Paterson, and M. D. de Jonge, "Fresnel coherent diffractive imaging," *Phys. Rev. Lett.*, vol. 97, no. 2, p. 025506, 2006.
- [129] B. Abbey, L. W. Whitehead, H. M. Quiney, D. J. Vine, G. A. Cadenazzi, C. A. Henderson, K. A. Nugent, E. Balaur, C. T. Putkunz, A. G. Peele, G. J. Williams, and I. McNulty, "Lensless imaging using broadband X-ray sources," *Nat. Photon.*, vol. 5, no. 7, pp. 420–424, 2011.
- [130] S. Witte, V. T. Tenner, D. W. Noom, and K. SE Eikema, "Ultra-broadband extreme-ultraviolet lensless imaging of extended complex structures," Preprints, arXiv:1302.6064 (2013).
- [131] H. N. Chapman, "Phase-retrieval X-ray microscopy by Wigner-distribution deconvolution," *Ultramicroscopy*, vol. 66, no. 3, pp. 153–172, 1996.
- [132] P. Thibault, M. Dierolf, A. Menzel, O. Bunk, C. David, and F. Pfeiffer, "High-resolution scanning X-ray diffraction microscopy," *Science*, vol. 321, no. 5887, pp. 379–382, 2008.
- [133] I. Peterson, B. Abbey, C.T. Putkunz, D.J. Vine, G.A. van Riessen, G.A. Cadenazzi, E. Balaur, R. Ryan, H.M. Quiney, I. McNulty, A.G. Peele, and K.A. Nugent, "Nanoscale fresnel coherent diffraction imaging tomography using ptychography," *Opt. Express*, vol. 20, no. 22, pp. 24 678–24 685, 2012.
- [134] O. Shapira, A. F. Abouraddy, J. D. Joannopoulos, and Y. Fink, "Complete modal decomposition for optical waveguides," *Phys. Rev. Lett.*, vol. 94, no. 14, p. 143902, 2005.
- [135] I. Robinson and R. Harder, "Coherent X-ray diffraction imaging of strain at the nanoscale," *Nat. Mater.*, vol. 8, no. 4, pp. 291–298, 2009.
- [136] M. C. Newton, S. J. Leake, R. Harder, and I. K. Robinson, "Three-dimensional imaging of strain in a single zno nanorod," *Nat. Mater.*, vol. 9, no. 2, pp. 120–124, 2009.
- [137] W. Yang, X. Huang, R. Harder et al. (2013, Apr.). Coherent diffraction imaging of nanoscale strain evolution in a single crystal under high pressure. *Nat. Commun.* [Online]. vol. 4, p. 1680. Available: <http://dx.doi.org/10.1038/ncomms2661>
- [138] M. Holt, R. Harder, R. Winarski, and V. Rose, "Nanoscale hard X-ray microscopy methods for materials studies," *Annu. Rev. Mater. Res.*, vol. 43, no. 1, pp. 183–211, 2013.
- [139] D. Gabor, "A new microscopic principle," *Nature*, vol. 161, no. 4098, pp. 777–778, 1948.
- [140] I. McNulty, J. Kirz, C. Jacobsen, E. H. Anderson, M. R. Howells, and D. P. Kern, "High-resolution imaging by Fourier transform X-ray holography," *Science*, vol. 256, no. 5059, pp. 1009–1012, 1992.
- [141] S. Kikuta, S. Aoki, S. Kosaki, and K. Kohra. (1972). X-ray holography of lens-less Fourier-transform type. *Opt. Commun.* [Online]. 5(2), pp. 86–89. Available: <http://www.sciencedirect.com/science/article/pii/0030401872900053>
- [142] S. Eisebitt, J. Lüning, W. F. Schlotter, M. Lörgen, O. Hellwig, W. Eberhardt, and J. Stöhr. (2004, Dec.). Lensless imaging of magnetic nanostructures by X-ray spectro-holography. *Nature*. [Online]. 432(7019), pp. 885–888. Available: <http://www.nature.com/nature/journal/v432/n7019/abs/nature03139.html>
- [143] T. Latychevskaia, J.-N. Longchamp, and H.-W. Fink, "When holography meets coherent diffraction imaging," *Opt. Express*, vol. 20, no. 27, pp. 28 871–28 892, 2012.
- [144] T. Popmintchev, M.-C. Chen, D. Popmintchev, P. Arpin, S. Brown, S. Ališauskas, G. Andriukaitis, T. Balčiūnas, O. D. Mücke, A. Pugzlys, A. Baltuška, B. Shim, S. E. Schrauth, A. Gaeta, C. Hernández-García, L. Plaja, A. Becker, A. Jaron-Becker, M. M. Murnane, and H. C. Kapteyn, "Bright coherent ultrahigh harmonics in the keV X-ray regime from mid-infrared femtosecond lasers," *Science*, vol. 336, no. 6086, pp. 1287–1291, 2012.
- [145] J. Miao, T. Ishikawa, B. Johnson, E. H. Anderson, B. Lai, and K. O. Hodgson, "High resolution 3D X-ray diffraction microscopy," *Phys. Rev. Lett.*, vol. 89, p. 088303, 2002.